Photoluminescence Based Semiconductor Defect Detection

An Honors Thesis for the Department of Physics and Astronomy

Robert Rockmore

Advisor: Professor Thomas Vandervelde

2014

Acknowledgements:

I would like to thank my thesis advisor Professor Tom Vandervelde for providing resources and guidance throughout this research. I would also like to thank the graduate students in his lab who have answered all my questions or helped me in other ways, specifically Nicole Pfiester Latham, Chandler Downs, and John Chivers. I would especially like to thank John for performing the photolithography and deposition for the microPL test sample and helping me out with the photolithography mask design.

Abstract: In this thesis, a characterization system for semiconductor materials was designed, fabricated, and tested. The capabilities of this setup include measuring photoluminescence emission at a single location of a sample, as well as performing spatially resolved “micro-photoluminescence” measurements throughout a region on the surface of the sample. A number of Gallium Arsenide semiconductor samples were examined in order to validate this testing setup. A Gallium Arsenide sample with known features was fabricated and tested using the spatially resolved imaging capability in order to determine the minimum defect and feature sizes that could be detected. After performing a number of different spatially resolved photoluminescence tests on this sample, photoluminescence blocking features of as small as 10 microns were detected (the smallest of the fabricated features), and the effective focused laser spot size was determined to be on the order of 100 microns. Optimal testing parameters and settings for both standard and spatially resolved PL were determined experimentally. This setup can be used to characterize the relevant performance characteristics, such as material uniformity, defect location, and variations in doping concentration in semiconductor materials for use in photovoltaics and other devices.

Table of Contents

I. Background.....5

II. Development of Testing Setup.....8

1. Standard Photoluminescence.....8
2. Micro-Photoluminescence.....20

III. Testing Methodology.....28

1. Standard Photoluminescence.....28
2. Micro-Photoluminescence.....29

IV. Results and Analysis.....31

1. Standard photoluminescence.....31
2. Micro-Photoluminescence.....38

V. Conclusions and Future Work.....58

Appendix.....60

I. Standard Photoluminescence Code.....60

II. Micro-Photoluminescence Code.....64

Bibliography.....70

I. Background

1. Motivation and Theory

Semiconductor devices have a multitude of uses in modern society, from computing to power generation, detection, and lighting. Solar power from photovoltaic cells is an important area for modern power generation, and improving the efficiency and performance of these cells is one of the main focuses of research in this area. Therefore, being able to characterize the properties of the semiconductor materials used to make these photovoltaic cells is of the utmost importance.

The periodic lattice structure of semiconductors gives rise to an energy band structure that contains a characteristic energy gap between the valence and conduction bands. This band is an area where there are no electronic states available for the electrons, and typically ranges from 1-2 eV for a semiconductor. This band gap is dependent on a number of different semiconductor properties. Therefore, being able to measure the characteristics of the band gap and related band structure allows us to determine information about the properties of the semiconductor material itself. Gallium Arsenide is one such semiconductor material, and has a lattice made up of both Gallium and Arsenic atoms.

Conduction in semiconductors is the result of not only electrons as in normal metals, but also by "holes," or available states in the valence band of atoms in the lattice. One type of these two charge carriers is given preference in a semiconductor material by doping, whereby impurities are intentionally added to the lattice. Donor impurities are atoms of an element that contains an additional electron when compared with the semiconductor element. The other electrons in this dopant form the lattice bonds, while the additional electron is free to move about the lattice. This is known as N type doping, and results in additional energy states just below the conduction band edge, typically separated by gaps on the order of .01 eV. This means that at typical thermal energy k*T (where k is the Boltzmann constant), the additional electrons can be elevated to the conduction band[1].

The other form of doping is known as "P-Type Doping," and adds acceptor impurities. These contain one fewer electron compared to the semiconductor atoms. The electrons that the dopant does have bind with other atoms in the lattice, but the dopant's lack of an electron means that there is one covalent bond that will only have one electron instead of the two required. This creates a "hole" where another electron can go. As electrons move to fill these holes, the holes

themselves are viewed as “moving” through the semiconductor, and therefore “carrying” a positive charge (although the holes themselves are not actually distinct particles as electrons are). These impurities add additional states just above the valence band that electrons can fill up at room temperature similar to the donor impurities[1].

Unintentional impurities can also add undesired states in the bandgap. These midgap states can reduce the performance of semiconductor devices, and therefore detecting characterizing them is important. Other potential issues with semiconductors are dislocations in the actual lattice structure, whether because of defects or because of mechanical stresses. These dislocations can affect charge carrier transport, which is detrimental for solar cell performance. In a solar cell, the charge carriers should be transported as efficiently as possible[2].

One major technique to measure these various properties of semiconductors is known as photoluminescence. When light strikes the semiconductor material, electrons in the valence band are elevated to the conduction band, provided the incident light is of a wavelength whose photon energy is greater than or equal to the band gap energy. The electron then undergoes nonradiative relaxation through interactions with lattice phonons (whereby its wavevector changes) until it arrives at the bottom of the conduction band. At this time it drops down to the valence band, emitting light of a wavelength equal to the band gap energy. The intensity of this emission is dependent on material properties, as well as the intensity of the incident light. Unlike the excitation laser, the emitted light is not coherent or collimated, but rather emitted more or less isotropically. By detecting the emitted spectrum, information can be determined about the properties of the sample. The presence of states in the band gap from impurities will shift the wavelength of PL emission. Time resolved PL uses short laser pulses to excite the carriers, and can then be used to observe time dependent properties such as recombination rates and carrier lifetimes[3].

Another major type of photoluminescence testing is micro-photoluminescence or “microPL,” also called spatially resolved photoluminescence. This technique takes photoluminescence measurements at many locations on a sample, which can show a great deal of information about the surface uniformity of a sample, as well as local areas of defects or undesirable properties[3]. For example, someone who wishes to use a semiconductor wafer for a photovoltaic device can image the surface and locate areas of lower emission at a certain

wavelength, which may be evidence of defects in the material. This information can then be used to determine which part of the wafer would best be used for the device fabrication.

A photoluminescence system consists of a few major components. The first is a coherent light source such as a laser, which provides the radiation for electron excitation. The second major component is a spectrographic device to analyze the spectrum of the emitted light. In a basic PL setup, this often takes the form of a monochromator connected to a photodetector or photomultiplier tube. A monochromator takes the emitted spectrum as input, and only permits a user selected variable wavelength as output to the detector. This allows a PL spectrum to be assembled by scanning through the specified wavelength range.

MicroPL systems are more complicated, and more varied in design. Some, such as the system here, use a precision XY stage to physically move the sample and take a normal PL spectrum at each location. Other systems keep the sample in one place and move the laser with a mirror galvanometer or other similar device. The advantage of the faster galvanometer based system over the slower moving stage system is that the laser spends much less time at each location, which reduces the chance for laser induced sample degradation[3]. However, such systems require a comparably fast method of spectral analysis. Monochromators rely on mechanical rotation of diffraction gratings or prisms to scan through spectra, which also limits the speed of systems containing them. CCD based spectrometers have much faster spectrum acquisition times, but are more expensive. More recently, CCD cameras have been used to image the entire sample simultaneously, using a laser that has its beam expanded to illuminate the whole sample as a light source[2]. One such system is capable of 160 micron resolution, with 20 second imaging times for the entire sample[4]. Some of these systems can are capable of imaging the entire sample multiple times a second (this can also be accomplished with a galvanometer based system as well). Confocal microscopy systems allow for depth resolution of PL results, and can also overcome the loss of resolution due to spatial carrier diffusion[3].

The testing system designed for this research utilizes and XY stage to produce spatial resolution. Similar systems have been used in the past, but have used a monochromator fixed at a single wavelength instead of scanning, as in this project [5]. This is a faster method of imaging than the system designed here, but loses information about the actual wavelengths of the peaks, which are important for measuring band gap energy.

II. Development of Testing Setup:

1. Standard Photoluminescence Setup

The experimental setup was first developed for standard photoluminescence testing. There are two major components of this setup: the physical hardware and optical elements on the optical table (including the electronics that interface with the computer), and the software that runs the testing and provides an interface for the operator. This software interface is was primarily developed in Labview, although the laser power was monitored using software provided by Thorlabs, the manufacturer of the power meter. Other software provided by the manufacturers of the devices used was employed for verification of various elements in the setup, but for the most part these were not used to conduct tests (with the exception of the aforementioned power meter software).

The majority of the components that were used to make this setup were already present in the laboratory from previous attempts at making a photoluminescence setup that had been more or less abandoned partway through the development process. The primary laser used was a JDSU 1145P helium neon laser with a measured maximum output power of approximately 22 mW and a wavelength of 632.8 nm. For noise reduction, a Thorlabs MC1000A optical chopper was used, along with an Anfatec AMU 2.4 PCI lockin amplifier. The optical chopper was placed in the path of the laser beam to convert the otherwise time invariant laser intensity into a pulsed signal. The optical chopper is capable of being controlled manually using the control unit. It is also capable of synchronizing its frequency to a reference input signal from an external source. In order to better integrate as many controls as possible into the Labview interface, I elected to control the optical chopper using the "reference out" signal output on the lockin amplifier card. This allows the frequency to be set directly by the computer containing the lockin amplifier card. The alternative method is to connect the "Ref output" on the chopper console to the reference signal input on the lockin amplifier. The lockin amplifier takes the signal from the detector and multiplies it by the reference signal. This signal then passes through a low pass filter where it is demodulated, returning the amplitude of the input signal and the phase difference between the reference and input signals (not used here). In this way any signals that are not very close to the reference frequency (such as those as a result of noise) are removed, significantly reducing the noise level. There are several parameters available to be controlled on the lockin amplifier, namely the time constant of the low pass filter used for demodulation, and the roll-off (in

dB/octave). This describes how the signals that pass through the filter roll off as the frequency gets farther from the reference frequency. The time constant determines the cutoff frequency below which the filter will allow signals to pass. For most of the testing conducted, the roll off was set to 24 dB/octave (the maximum value for this lockin amplifier), and the time constant was set to 20 ms. I arrived at these values after extensive experimental testing upon completion of the setup; these were the values that provided the best photoluminescence spectra.

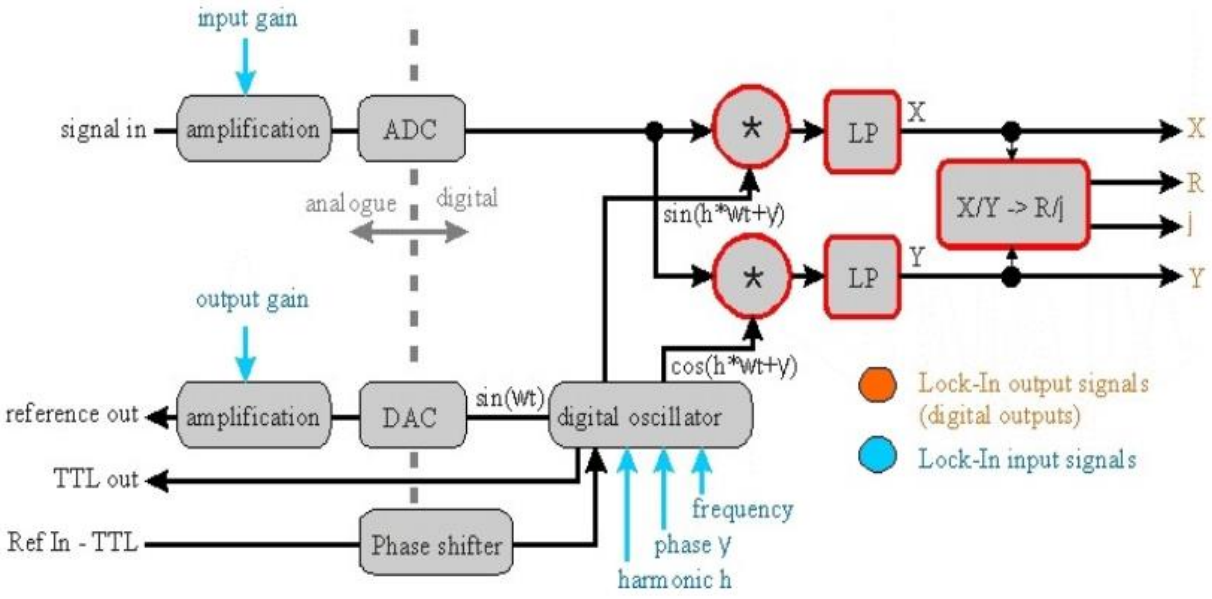

Figure 1: Diagram of inputs, outputs, and basic internal operation of Anfatec Lockin amplifier. The "reference out" channel here was used to send the reference signal to the optical chopper, while the "signal in" input was connected to the photoreceiver output. "LP" denotes the low pass filter stages for demodulation, while the top and bottom asterisk represent multiplication of the input signal by the reference signal and 90 degree phase shifted reference signal, respectively. This yields a number of outputs, including the amplitude R and phase shift (between reference and input signal) j. The R output was what was used in this testing.[6]

Two different photoreceivers were selected for detection: the New Focus 2151 and 2153 model femtowatt photoreceivers. The 2151 model has a silicon detector with a detection range of 300-1050 nm, while the 2153 model uses an InGaAs detector with a range of 800-1700 nm. Both models feature 2 gain modes: AC low, AC high, and DC low. These detectors produce a voltage as output that is related to the incident optical power by equation (1), where V is the output voltage, P_{in} is the optical power incident on the sensor, R is the responsivity of the photodetector in Amps per Watt, and G is the gain of the amplifier in Volts per Amp[7].

$$V = P_{\text{in}} * R * G \quad \textbf{(1)}$$

The responsivity is wavelength dependent. As these detectors are not calibrated units, the exact responsivity is not known, so relative light intensities at different wavelengths cannot be compared. However, as the primary purposes of this setup are to determine the wavelengths of peaks (in standard PL measurements) and compare the intensities of peaks of the same wavelength at different spatial positions (microPL), the fact that the responsivity varies somewhat with wavelength is not an issue. The typical maximum responsivities are .5 A/W at 900 nm for the 2151 detector and 1.0 A/W at 1600 nm for the 2153 detector. The gain G is independent of wavelength and depends only on amplifier gain settings, which are the same for both of the detectors. The AC and DC low gain is $2x10^{10}$ V/A, while the AC high gain is $2x10^{11}$ V/A. Although the AC and DC low gain have the same value, they differ in that the AC gain settings have a high pass filter with a cutoff below approximately 30 Hz, while the DC gain setting does not attenuate DC signals. Since an optical chopper is being used to modulate the laser light (and therefore the PL emission as well), the AC gain was chosen to further reduce noise caused by ambient light that has a time independent intensity.[7]

As these photoreceivers simply measure intensity of incident light and not its wavelength, a wavelength selection device was required to step through each wavelength in the desired range sequentially so that the emission intensity could be measured. A Spectral Products CM110 monochromator was used for this purpose. The light to be investigated enters through the entrance slit, where it is focused by a series of mirrors onto a diffraction grating that results in a dispersion effect. This grating causes light of different wavelengths to reflect off of it at different angles, representing the frequency domain of the light in the spatial domain. A narrow band of this wavelength range is selected when it is passed through a narrow exit slit. The range of the wavelength band that passes through the monochromator is determined primarily by the exit slit width, as a narrower slit will let a smaller portion of the now spatially extended spectrum pass through. The entrance slit width also affects the wavelength resolution because of imaging effects[8]. There is an inherent limit in resolution of the grating used in the monochromator, but this is typically on the order of Angstroms, and will therefore not be the limiting spectral resolution[9]. The wavelength that passes through is selected by changing the angle of the diffraction grating with respect to the mirrors that focus the light to and from the entrance and exit slits. The basic optical path of the CM110 is shown in Figure 2.

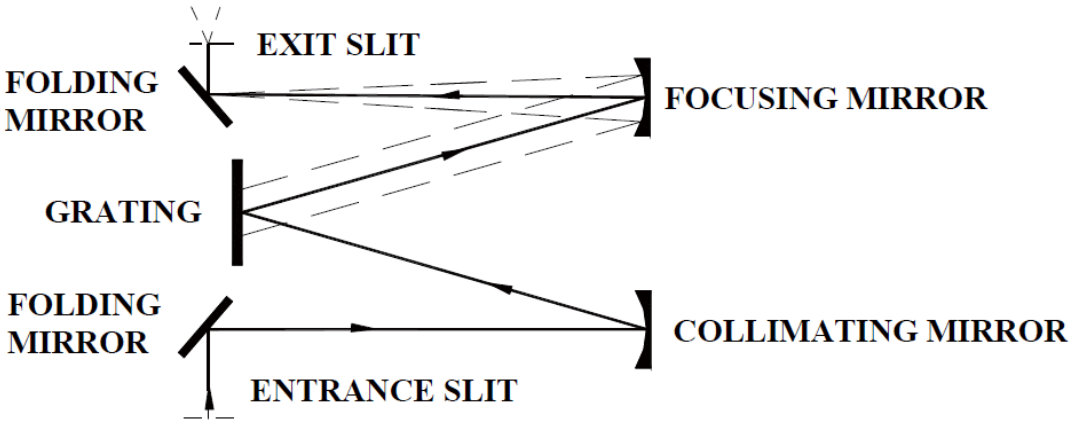

Figure 2: Internal layout of the CM110 Czerny-Turner type monochromator, viewed from above. The grating is rotated by a computer controlled motor in order to select a specific wavelength (actually a narrow band).[9]

The photoreceiver was mounted directly at the exit slit of the monochromator. However, before aligning the photoreceiver, the rest of the optical elements in the PL setup were assembled and aligned. The final optical path consisted of two main stages: the laser stage, and the detection stage. The laser stage includes of everything from the laser to the sample, while the detection stage includes everything from the sample to the detector. The light passing through the laser stage is monochromatic, while the light passing through the detection stage contains both reflected laser light and photoluminescence emission.

The laser stage starts with the HeNe laser. Directly after the laser is an adjustable neutral density filter for laser power attenuation, followed by the optical chopper. A series of two mirrors directs the laser towards the sample. After the second mirror is a plano convex lens (Thorlabs LA1417) with an effective focal length (EFL) of 150 mm and a back focal length (BFL; the distance from the flat face of the lens to the focal point on that side) of 145.2 mm. This lens serves to focus the laser to a smaller spot for greater PL intensity and higher spatial resolution.

There are two ways to calculate the size of the laser spot. The first is through classical ray optics, ignoring the wavelength of the light. This only depends on the divergence angle of the laser and the focal length of the focusing lens:

$$S = \theta * f \quad \textbf{(2)}$$

Here S is the focused spot size, θ is the full angle divergence of the laser, and f is the effective focal length of the lens[10]. The JDSU 1145P laser has a full angle divergence of 1.15 mrad (+/-3%) [11], and the LA1417 lens has an effective focal length of 150mm. This yields a minimum spot size of 172.5 microns at the focal point of the lens. However, the laser beam more closely resembles a Gaussian beam than a series of classical rays. Even with a perfectly collimated beam hitting the lens, there will be a minimum spot size that depends on the wavelength of the light. This spot size can be approximated by the following equation:

$$S = \left(\frac{4\lambda}{\pi}\right)\left(\frac{f}{x}\right) \quad \textbf{(3)}$$

S is once again the spot size, but here it is the diameter of the Gaussian beam waist, the narrowest part of the Gaussian beam**.** A Gaussian beam has a cross sectional electric field intensity that is given spatially by a Gaussian function. As Gaussian distributions have infinite spatial extent, the beam width at the waist is defined as the diameter of the beam that extends until the intensity has dropped off to $1/e^2$ of the peak value (which is found at the axis of propagation). F is the focal length of the lens, and x is the diameter of the lens that is illuminated by the beam. This assumes a collimated beam, while the beam of the helium neon laser used has a non-zero divergence, making it less than perfectly collimated. Therefore, this equation will only provide a lower limit on the spot size that will not be fully realized with this setup[12]. The value of x was calculated from the divergence of the laser and the optical path length between the laser and focusing lens. More precisely $x = L * \mathrm{Tan}[\frac{\theta}{2}]$, where θ is the full angle divergence of the laser and L is the optical path of the beam (including its travel through the two reflecting mirrors) and was measured to be approximately 1635 mm. This yields a spot diameter of approximately 64 microns, which is smaller than the classically calculated value. This means that in its current configuration, the focused laser spot size is limited by primarily by the laser divergence angle, and not on wavelength dependent effects.

However, the laser spot size does not completely determine the spatial resolution for a PL setup. Photoexcited carriers can typically diffuse on the order of 1-10 microns, which leads to an emission area that is larger than the laser spot, regardless of how focused it is[3].

In developing the setup, the sample stage was initially placed at the focal point of the lens, approximately 145.2 mm from the flat face of the plan-convex laser focusing lens. However, the best performance of the system was obtained at a different focal location which will be discussed later in this section.

The “detection stage” of the system runs parallel to the laser beam as it leaves the laser. This allows the system to be smaller by folding it back on itself. The detection stage consists of the optics that focus the photoluminescence emission through the monochromator into the photoreceiver detector. The focused laser forms an angle of approximately 65 degrees with the sample. This ensures that specular reflection of the laser off of the sample surface does not enter the detection system, but is instead diverted off to the side. The photoluminescence emission is not coherent and is not emitted in the direction of laser reflection, but is instead emitted spherically from the optically excited area. Because the PL intensity is low, this emission must be focused onto the monochromator.

The focusing was accomplished using two Thorlabs LA1050 plano-convex lenses, with an effective focal length of 100 mm and back focal length of 93.6 mm. These two lenses were placed in series as shown in Figure 3, with the flat faces facing opposite each other. The lens closest to the sample serves to collimate the PL emission so that it can be transmitted the distance to the second lens without loss due to divergence. Since the PL emission is roughly a spherical wave, the intensity will decrease proportional to the inverse square of the distance to the sample. Therefore, for a given lens diameter, a lens that can be placed closer to the sample will take up a larger solid angle of this sphere, and thereby absorb a larger percentage of the emitted PL light. With this reasoning in mind, a lens with a shorter 100 mm focal length was chosen for collimation, since a point source at the focal point of a converging lens will be focused at infinity[13]. However, the PL emission area is not a point source, so the collimation will not be perfect. The nearly collimated light that leaves this lens enters the second plano-convex lens 250 mm away, where it is focused onto the monochromator entrance slit. Directly next to the monochromator exit slit is the photoreceiver. It was placed flush with the collar around the monochromator slit to prevent stray light from striking the photodetector itself.

The setup also features a few modular components on magnetic mounts so that they can be added or removed from the optical path with ease. The first of these is a Thorlabs S120C

power sensor. This sensor, with an operating range of 400-1100 nm, is inserted directly after the neutral density filter in the optical path, and is used to measure the power output of the laser. The second removable component is an additional mirror to insert a different laser into the optical path. This mirror obscures the HeNe laser (which would be turned off in this case) and aligns a beam from a 20 mW 405 nm diode laser in place of the HeNe beam. This laser was not used for the more rigorous testing that will be discussed here, but it was aligned and preliminary testing was performed. The shorter wavelength (and therefore higher energy) of the diode laser allows materials with a larger bandgap to be investigated.

The optical configuration is show in Figure 3. Initially, the samples were held by a simple slide holder. Once the setup was expanded to do microPL measurements, the sample stage was replaced with the movable XY stage in the same location.

The alignment and focusing of the system was a multi-step process, and underwent several revisions throughout this research in response to various test results. The first step was to align the laser beam onto the sample. This was done by changing the angles and positioning of the mirrors, as well as the angle of the laser itself. Once the spot was on target, the focusing lens was added with the sample at approximately the focal point of the lens. The monochromator position was chosen based ease of access; since the emission is collimated before being sent to the monochromator (where it is decollimated), it should not decrease in intensity significantly over a distance of a few hundred mm. Placing the monochromator farther from the optics allows for easier removal and access to the photoreceiver without accidentally altering the alignment of the mirrors. This is important, as the choice of which of the two detectors is used is dependent on the material being studied (removal is also necessary to replace the battery for the unit). The detector itself was mounted with a right angle mount that allows it to be rotated to visually inspect the diode while maintaining a constant height, which is convenient for alignment purposes.

The focusing of the emission onto the monochromator entrance slit was one of the most important components of the development process. With these elements out of focus, measured PL results were poor and sometimes not present at all. The placement of the collimating lens and focusing lenses were determined experimentally and visually rather than based on theoretical values. An attempt was made to align the system by putting the sample and monochromator

entrance slit at the focal points of the collimating and focusing lenses, respectively. However, the results obtained with this configuration were not ideal. The experimental focusing was performed using a laser and a piece of white paper in place of a sample. This white paper provided a diffuse reflection of the laser, which is similar to the PL emission in that it is not anisotropic or coherent, but rather more or less constant over the entire hemisphere of reflection. More importantly, it is in the visible range and much more intense than PL emission, making it possible to see the path of the light through the system visually. The goal was to have a focused spot at the monochromator entrance slit that had the highest intensity and smallest spot size possible, which would result in a higher intensity on the detector. First, the collimating lens was placed approximately at the focal point of the lens (100mm). Because the samples tested were typically around a millimeter thick when mounted on a slide, this position was moved slightly to approximately 102 mm. The height of the collimating lens was set so that the center was at the same height as the laser spot and the monochromator entrance slit (these had previously been aligned to be at the same level). The focusing lens was placed in the path of the now collimated laser light from the diffuse reflection. Using another piece of white paper, the height of the collimating lens was adjusted so that its aperture coincided with the beam of collimated light from collimating lens. The entrance slit on the monochromator was pulled out partially so as to completely block the entrance. This allows the focused spot to be seen where it would be entering the monochromator slit (and therefore not visible). The focusing lens was then moved along the detection axis (formed by the sample stage and monochromator entrance slit) until the spot was at its most intense and spot size was at a minimum.

In order to align the detector, the monochromator was set to allow all wavelengths through by rotating the grating such that the zero order diffraction peak (under which the ray is specularly reflected) emerges from the exit slit. With the piece of white paper still in place, the focused image of the diffusely reflected laser light can be clearly seen through the exit slit. Alignment of the detector simply consists of adjusting the height and lateral position until this light directly strikes the detector. Once this positioning was determined, the detector was rotated fully so that it lay flush against the monochromator.

The laser focusing lens was added last, and was placed so the sample was at approximately the focal point of the lens. However, this was later changed slightly for various

reasons, such as to account for the sample thickness and also to avoid the focusing lens housing from blocking a portion of the collimated PL emission.

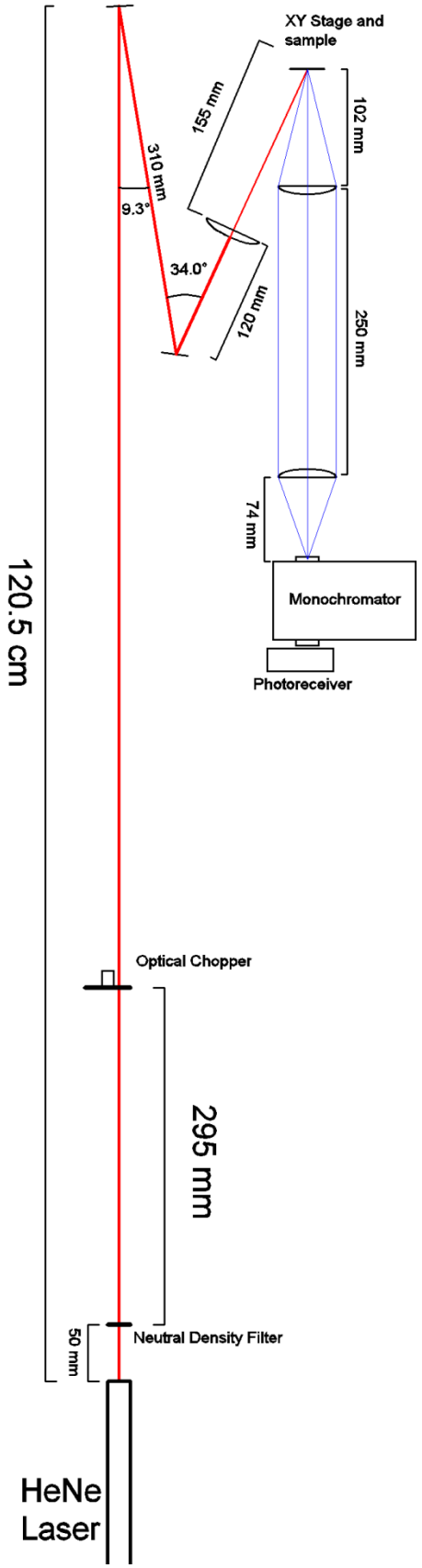

Figure 3: This diagram shows the final optical path. All distances and angles are to scale, as are mirror and lens angles and positions (the lens thicknesses are not to scale). All three lenses used have 2 inch diameter. The size of the laser, monochromator, and photoreceiver are not to scale. The red line traces the laser path from the aperture to the sample, while the blue lines show the path of the incoherent PL emission through the collimating and focusing lenses. The angle formed between the incident beam and sample is approximately 65 degrees, although the precise angle will vary depending on sample orientation. The laser light that is specularly reflected off of the sample is directed into a closed black aperture to prevent it from affecting the results or causing potential eye damage. The optical power meter (not shown) is placed on a removable magnetic mount between the neutral density filter and optical chopper in the optical path.

The code for the standard PL setup was developed using the Labview software. This allows the computer to interface with the various devices easily and integrate them into a single program and unified user interface. Some of the standard PL code used for this setup had been developed previously by a group in the lab that had previously attempted to make a photoluminescence setup. These were Emir Salih Magden, Victor Minden, and Corey Shemelya. I then modified this code to add functionality and remove some unnecessary parts, as well as create a better file output system. However, prior to using the code, the instruments had to be set up to interface properly with the computer system. The instruments that interface with the computer either directly or indirectly are the monochromator, the lockin amplifier, the photoreceiver, and the optical chopper. Both the photoreceiver and optical chopper are managed by the lockin amplifier as discussed previously. The monochromator interfaces with the computer through an rs232 serial port. Through this interface, the computer can send a number of different commands. The primary commands used in the PL code are the "GOTO" command, which has the monochromator scan to a specific wavelength by rotating the diffraction grating the required number of degrees (this is managed internally within the monochromator), and the "STEP" command, which moves the grating an amount that will shift the output wavelength by the amount specified. The monochromator related parameters in the PL code are the starting wavelength, ending wavelength, and step size. The GOTO command is used to scan the monochromator to the starting wavelength, while the STEP command is used to step through each wavelength in intervals equal to the step size.

The lockin amplifier settings are directly accessible through the interface for the PL code. In this way, the lockin amplifier gain, roll-off, phase, time constant, and chopper frequency can be adjusted. There is also a "PLL" (phase locked loop) option to allow the user to specify chopper frequency through the chopper control box (this was kept turned off).

The operation of the optical chopper and photodetector is fully integrated into to that of the lockin amplifier. As previously discussed, the lockin amp has a number of outputs that can be addressed by the computer. The output used by the PL code is the amplitude output, or R in Figure 1. The goal of the setup is to measure the PL emission at each wavelength step. In order to improve results, a time averaging is built into each detection step. This takes multiple measurements of the detector voltage at specified time intervals. The user specifies a total sample time and the number of desired samples during this time interval. At each wavelength

step, the computer reads the photodetector voltage (via the lockin amp) and then waits an amount of time equal to (sample time)/(number of samples). These measurements are then averaged together for a reading with less uncertainty. Assuming random error, the uncertainty on these measurements will be proportional to 1/sqrt(N), so a larger number of samples will result in a more accurate value. This average value is then stored in an array, along with the current wavelength. This array is graphed on the front panel of the Labview VI (Virtual Instrument), with wavelength on the X axis and detector voltage on the Y axis. The second graph performs a 3 point moving average on the data and graphs those values. When the "Output data to file?" option is enabled, the array is also saved in a text file. Additionally, a header is created for this text file that includes all of the relevant settings and parameters, such as starting and ending wavelengths, step size, sample time, etc. The full list of variables that are included in the header can be found in the Labview code in the appendix. Finally, a timing system was added that calculates and reports the total duration of the test in seconds.

The validation of the standard PL setup was achieved primarily by using the HeNe laser as a source of known wavelength. A piece of white paper was used again as a source of diffuse reflection. If the system is aligned well and the monochromator is calibrated, the measured spectrum for this source should be a single sharp peak at approximately 633 nm. Because the diffuse laser light is much brighter than any PL emission, small entrance and exit slits were used for this testing, as well as the neutral density filter to avoid saturating the detector. Because the monochromator uses a diffraction grating, there are higher order peaks that can potentially interfere with data. When the monochromator grating is set to an integer multiple of the wavelength of the laser, a significant amount of light (compared to typical PL emission intensity) will be let through. For example, scanning between 1000-1500 nm while using a HeNe laser as a source will result in a peak at approximately 1266 nm. This can be an issue if the expected band gap of the material you want to study is close to that peak. In that case, using the 405 nm violet laser will produce a peak at 1215 nm, which may be sufficiently far so as to not interfere with the PL peak of interest. These higher order peaks can be removed by using a double monochromator, which is essentially two monochromators in series. In this case both monochromators are scanned to the same wavelength. If the first monochromator is scanned to a wavelength that is an integer multiple of the laser wavelength, it will let through the higher order laser peak. This weaker higher order peak will then create a second higher order peak in the second

monochromator, but the intensity will be much less than with a single monochromator. However, dual monochromators reduce the intensity significantly, and can make it difficult to detect weaker PL signals[9]. For this reason, a single monochromator was used for this testing.

2. Micro-Photoluminescence Setup

The physical layout of the microPL setup is largely the same as the standard PL setup. The main addition is the two Zaber T-LSM025A motorized linear stages, which are used to move the sample in the X (horizontal) and Y (vertical) direction. These stages are arranged such that the vertical stage is attached to the moving portion of the first stage, so that the axis of movement of the second stage is perpendicular to that of the first. Figure 4 shows the configuration of the stages and the sample holder.

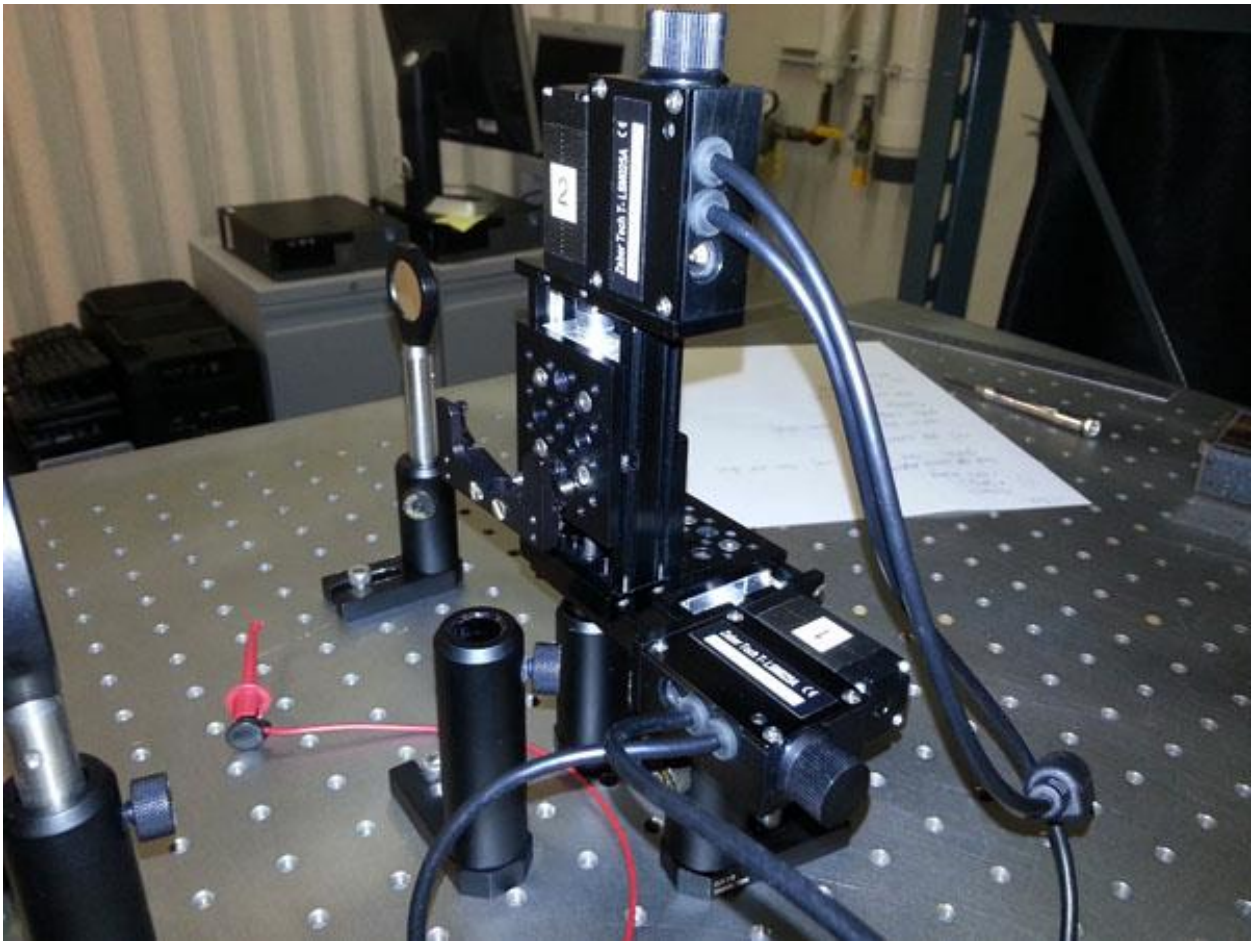

Figure 4: Two linear stages are combined to form the XY stage. The knobs allow for manual adjustment of the stages.

The T-LSM025A has a range of motion of 1 inch, an accuracy of 8 microns, and a repeatability of less than 1 micron. Accuracy is defined as the maximum possible error when moving between two positions when both positions are approached from the same direction. Repeatability is the maximum deviation in actual position when the stage is instructed to move to a target position 100 times (from the same direction). The motor receives movement commands in units of microsteps, which are equal to .047625 microns under default settings[14]. However, the actual accuracy is 8 microns, which is nearly 200 microsteps. The stages can be moved manually using the control knobs for initial positioning. More precise movements are achieved using computer commands. The computer communicates with the two stages via serial commands, with the two stages daisy chained together with a single serial connection. Each stage is therefore addressed according to its number (the X stage is addressed as device number 1, and the Y stage is addressed as device number 2).

The main idea of the microPL setup is to take individual PL spectra at many locations along the surface of a sample. The precision XY stage is used to advance the sample in both the vertical and horizontal direction while keeping the laser spot in the same place. In this way, PL measurements can be taken anywhere on a 1 inch by 1 inch square (limited by the stage movement range). The most logical way to subdivide the sample surface into separate measurement regions is in a grid pattern. PL measurements would then be taken at each square in the grid. However, this still leaves multiple choices of where on each square to take the measurement; one could choose a corner of the square, a point on the edges, or a point inside the square. For high resolution scans that are made up of grids of many squares this choice doesn't have a large effect beyond translating the locations on the sample that are being measured a distance less than or equal to the grid spacing. I chose to have the system take the measurements in the center of each square. The grid itself is defined by 4 coordinates: the minimum X and Y values and the maximum X and Y values. These define the overall size of the square grid. For the XY stages, these coordinates are given in units of microsteps. To allow for determination of the current position of the XY stage, I designed a simple program in Labview that queries each of the stages for their current position, and then displays these positions in microsteps. The manual control knobs on the stages allow the user to move the sample to the desired starting location, at which point this code is used to get the coordinates of that point in microsteps. The same procedure is repeated to get the coordinates of the desired ending location.

The microPL movement code responsible for stepping through this grid was designed first. Initially, the main input parameters for this code were the starting and ending X and Y coordinates, as well as the number of steps. Defining the number of steps initially instead of the step resolution was more convenient for testing on a larger scale with large movements and small numbers of steps, where specifying a resolution would result in divisibility and remainder issues. For a given set of start and end coordinates, the code will scan first along the horizontal axis and then the vertical axis, in increments defined by the number of steps. In order to measure PL in the center of each grid square both X and Y movements were split into two steps, with half of the desired X movement occurring prior to measurement, and half occurring after. Similarly, the first half of each Y step was made prior to each line of X scanning, and the second step was made after each line of X scanning was complete. Because measurements are taken in the center of each grid square, the specified boundaries of the sample testing region are larger than the region that is measured. However, for high resolution tests where the X and Y step size are smaller than the focused laser spot size (which is the case for most of the PL measurements here), the difference is not relevant because the laser excitation area will be large enough relative to each grid square to reach the region boundary.

The final version of the microPL code takes the desired step resolution in microns as input. Two different types of move commands were used: "move absolute" which moves the stage to a specific microstep index, and "move relative," which moves the stage a specified number of microsteps from its current position. The code sends the "move absolute" command with the initial X and Y coordinates to move the stages to the start of the region. The step size in microns is then converted into microsteps. The system takes half a Y step and half an X step (using the "move relative" command) to move it into position for the first measurement. After the first measurement is taken, it moves another half x step. The following loop is then repeated: ½ X step, PL measurement, ½ X step. The number of iterations of this X movement loop is determined by the total X range divided by the step size, rounded up. This means that there will be a slight overshoot when the step size is not an integer multiple of the total desired range. For high resolution testing this overshoot is minor. If the limits of the testing region are very strict and require undershoot instead of overshoot, the code can easily be altered to round down instead of up.

The next major obstacle of coding the microPL setup was synchronization. Because each PL measurement requires a physical movement of the stage, any wasted time can result in a significantly longer overall test for high scan resolutions. This makes precise synchronization of the steps of the microPL very important; even with a total overall time per step of 1 second (including PL measurement and movement), a 100 x 100 resolution test will take 2.8 hours, while a 200 x 200 test will take over 11. The travel time of the stage for small resolutions (on the order of tens of microns) is very small, but the XY stage itself does not natively report when each move command has been completed. Instead of using "wait until" timers, I followed each move command by a segment of code that queries the current position of the stage every millisecond while it is moving. Once it has arrived at the desired location, the next step in the code is initiated. In this way, unnecessary waiting is reduced without causing issues with synchronization (such as the PL measurement beginning when the sample is still moving). One of the main overall goals in designing the microPL code was to reduce the running time for a step as much as possible without significantly affecting the quality of the data.

The PL measurement portion of the code contains a number of differences from the standard PL code. First, the code was modularized and turned into a "subVI" in Labview, which turns the code into a functional object within the microPL code, with a series of inputs and outputs. These inputs are the same as those from the standard PL code, and most are simply passed through to the user interface of the microPL code. The outputs of this subVI are the array of wavelengths, the raw data, and the 3 point average data. At each position step, the PL spectrum is saved into another array, which eventually yields a 2D array (corresponding to spatial locations) made up of PL spectra of intensity vs. wavelength. However, the 3 point moving average output is sent to a peak detection function. The moving average filter reduces noise but will not change the position of a large peak made up of many sample points. The Labview function used for peak detection is the "Advanced Peak Detection" VI included in Labview. This function finds all of the peaks in the data that are above a certain specified threshold. It then reports the indices of these peaks in the initial array data, as well as the intensity of each peak. The microPL code takes this output and locates the maximum of these reported peaks (if multiple peaks are present) and saves the wavelength of this peak in one 2D array, and the intensity in a second 2D array. Each entry on this array corresponds to a single testing spot on the spatial PL grid. These arrays are saved in a text file, along with the raw data

of wavelength vs. intensity at each location. This results in very large text files of data, but it preserves all of the spectral data from the test. The 2D arrays can then be used to create colormap "pseudo-images" based on the intensity and wavelength data.

In order to validate and test the spatial resolution of the microPL setup, a test sample was designed and fabricated. The purpose of this sample was to simulate areas that contain defects by depositing a metal on the surface of a piece of N-type doped GaAs semiconductor wafer. The metal, being opaque at the laser wavelength, will block absorption by the GaAs at that location, preventing any PL emission from occurring. Two main shapes were deposited: squares, and lines. The lines allow for fast linear tests (scanning a single line in the X direction) to determine linear resolution, while the squares simulate spatially isolated defects to test 2D resolution. The following sizes of lines and squares were deposited: 1000 microns (no lines were used for this size because of their large size), 500 microns, 200 microns, 100 microns, 50 microns, and 10 microns. This pattern was designed and then used to make a photolithography mask in order to deposit chrome on the surface of a GaAs wafer. The design for the mask is show in Figure 5, while Figure 6 and Figure 7 show the finished sample after deposition.

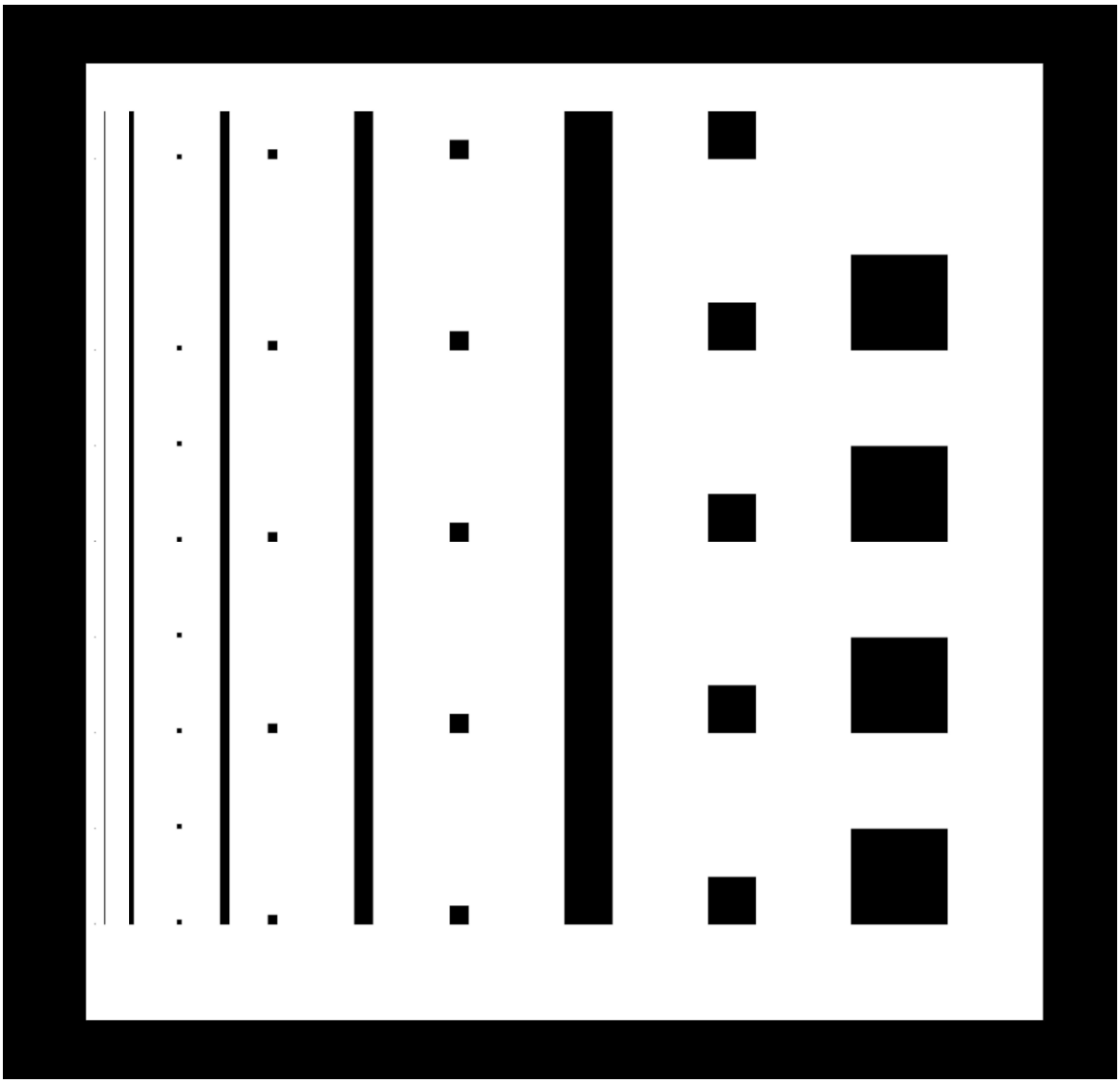

Figure 5: The photolithography mask shown here was designed in AutoCAD. The black areas represent areas that are to have chrome deposited, while the white areas are to be exposed semiconductor. The total size of the exposed semiconductor square is 1 centimeter. The farthest left squares (which are barely visible in this image) are 10 microns to a side. The following line is 10 microns wide, followed by a 50 micron line and 50 micron square. The next line and squares are 100 microns, followed by 200 microns, 500 microns, and finally 1000 microns for the largest squares.

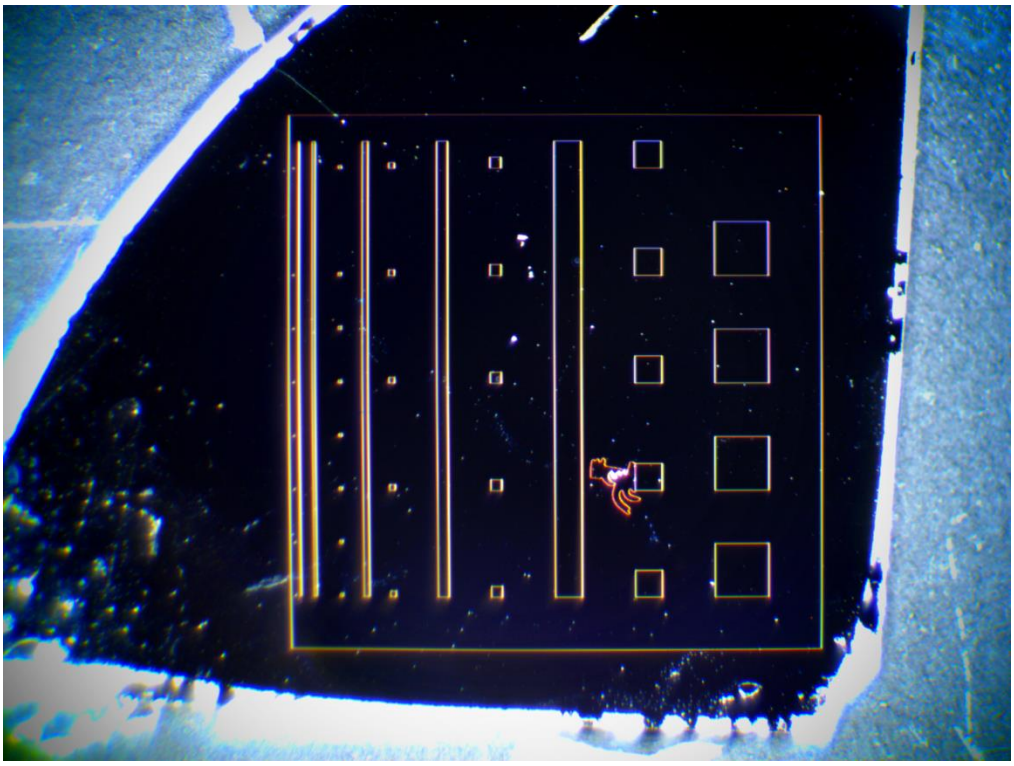

Figure 6: Top down image of the fabricated test sample. From this angle, it is difficult to differentiate between chrome and GaAs regions because the diffuse light source does not reflect directly off of the sample into the camera when viewed at this angle. Note the defect present on the second 500 micron square from the bottom. This will be discussed and analyzed in the results section.

Figure 7: This image was taken at an angle with a diffuse incandescent light source reflecting off the sample into the camera. This direct reflection allows us to differentiate the darker chrome areas from the lighter GaAs regions.

III. Testing Methodology:

1. Standard Photoluminescence Testing

"Standard" PL measurements are those taken at a single location on the sample. In this case the area producing PL emission is localized at the laser spot only. The following experimental procedure assumes focusing of the entire setup has been conducted as described in the previous section. Diagnostic tests were conducted during development of the characterization setup described previously to develop an ideal experimental procedure for routine testing. The following settings were used for these standard PL tests:

Main Settings:
Initial Wavelength: 500.00 nm, Final Wavelength: 900.00 nm,
Step Size: 1.0 nm
Sample Time: 10.00 ms, Number of Samples: 10,
Lockin Settings:
Time Constant: 6, Input Gain: 10, Roll-Off= 24 dB/octave,
Lockin Frequency: 100.00,
Phase: 0.000

10 samples with a 10 millisecond total sample time correspond to 1 sample per millisecond. An input gain of 10 corresponds to "normal" through the interface, while a time constant of 6 corresponds to 20 ms.

These measurements were performed on the fabricated GaAs test sample in a region in the upper right corner not coated with metal. The sample was placed in the XY stage (which remained stationary during the duration of the test). The ~22 mW continuous power Helium Neon laser was used for this testing, with the neutral density filter in place for attenuation of beam intensity. The laser power was monitored with the Thorlabs optical power meter before testing to ensure that the beam intensity had stabilized at its steady state value. The laser power was recorded immediately before testing. The purpose of this portion of the testing was to determine the effect of laser power and monochromator slit size on measured PL spectra. Two levels of laser power were investigated: approximately 2.66 mW, and approximately 5.0 mW. The laser power as measured by the sensor fluctuated slightly from test to test, most likely due to random noise. However, the power readings were sufficiently close to ensure valid results. The New Focus 2151 femtowatt photoreceiver was used for these tests, with a range of 300-1050 nm. The gain on the photoreceiver was set to "AC low," among the other two settings of "AC High" and "DC low." The expected bandgap of GaAs is 1.43 eV at 300K, which is approximately 867

nm[1]. Four different sizes of monochromator slits were used for these tests: .3 mm, .6 mm, 1.2 mm, and 2.4 mm. The same sizes were used for both the entrance and exit slits. Laser power was altered using the neutral density filter, which was rotated until the power meter read the desired power level. In order to minimize the effect of laser degradation of the sample area being examined, the testing was started with the lowest laser power (~2.66 mW). As in all other testing, the optical chopper controller was set so that "external in" option was enabled, so that the frequency could be controlled by the labview software through the lockin amplifier's signal output capability. To accommodate this, the PLL (Phase Locked Loop) function of the lockin amplifier was disabled. The wavelength range that was selected for these tests was from 500 nm to 900 nm. This is well within the range of the monochromator grating and the femtowatt photoreceiver that were used, and includes both the HeNe laser output wavelength (approximately 632 nm) and the expected GaAs emission wavelength in the 860-870 nm region. The 1200 grooves per millimeter grating was used (with a blaze wavelength of 500 nm), with a wavelength range of 330-1000 nm. Also available was a second grating with 600 grooves per mm, 1200 nm blaze, and a range of 800-3000 nm. This was not used for the GaAs testing.

For the standard PL testing, a region of the test sample that did not have metal deposited on its surface was chosen. The specific location was not recorded, but was used for all of the successive tests regarding the laser power and monochromator slit sizes. Prior to testing, the room lights were turned off and the computer monitors were covered with an opaque shroud. As previously mentioned, the wavelength scanning range was from 500 nm to 900 nm, which is within the center of the range of both the monochromator and detector. Each test was initiated by running the labview program for standard Photoluminescence ("PL.vi" in the appendix). After each test run the entrance and exit slits on the monochromator were swapped out for the next size, and testing was repeated. After all four slits had been tested at 2.66 mW, the laser power was altered to the higher power of approximately 5 mW and testing was conducted in the same manner for each of the four monochromator slit sizes.

2. **Micro-Photoluminescence Testing**

The microPL testing was conducted on a number of different GaAs samples. However, the general procedure was the same for each. First, the sample to be investigated was mounted on a glass slide with mounting wax using a hotplate. The slide was then placed in the clip mount of the XY stage. The power was then connected to the XY stage, and it was initialized by using the

manual control knobs to position each slide at its maximum travel distance (this zeroing is necessary for the system to determine its current position).

In order to specify the start and end points of the X and Y coordinates, the "MicroPL Positioning.vi" Labview program was used. This program reports the current X and Y coordinates of the XY stage. With the laser turned on, the manual control knobs were used to move the stage to the lower left corner of the desired testing region. Once the sample was in the desired location, the positioning VI was run, reporting the current coordinates. These were then entered into the "X start point" and "Y start point" fields of the MicroPL VI. The stage was then moved to the upper right corner of the desired region and the coordinates were again reported and entered into the "X end point" and "Y end point" fields. The peak threshold voltage was set to .004 volts. Since the typical noise level for these tests is consistently .001-.002 V, a threshold of .004 ensures that any peaks detected are safely outside of the noise region, and therefore highly likely to be actual emission peaks. PL settings were set to the values given in the previous section with the exception of wavelength range. For the high resolution GaAs tests, a wavelength range of 840-880 nm was used. This was determined from the peak locations that were measured in the standard PL test conducted on the sample immediately before MicroPL testing. The monochromator return delay was set to 100 ms, which was suitable for the wavelength range being investigated.

The X step size and Y step size were specified in microns and entered into their respective fields. These varied from test to test depending on the desired step resolution. Testing was conducted with the room lights turned off and monitors covered as before. These microPL tests typically took approximately 1 second per spatial step, and as many of the tests contained hundreds of lines of resolution in both vertical and horizontal dimensions, these tests took upwards of a dozen hours. Upon completion of a test, the total time in seconds was reported in the front panel of the VI. Directly after starting the VI, the number of X and Y steps were calculated based on the specified resolution, start points, and end points.

When tests were completed on a sample, the laser, detector, and optical chopper were turned off, and the power supply for the XY stage was unplugged. The fabricated microPL testing sample was kept in the nitrogen dry box when not being tested, and was promptly returned there after each test to avoid contamination.

IV: Results and Analysis

1. Standard Photoluminescence:

The first data that will be analyzed is the standard PL data, taken from the same GaAs sample with different slit widths and using different laser powers. The following data shows the relative peaks of both the reflected laser light and the PL emission for these varying parameters. The purpose of these tests was to determine the ideal settings for this particular sample, as well as determine some of the operating parameters of the setup, namely spectral resolution, signal to noise ratio, detector saturation, and the dependence of the quality of data on the incident laser power.

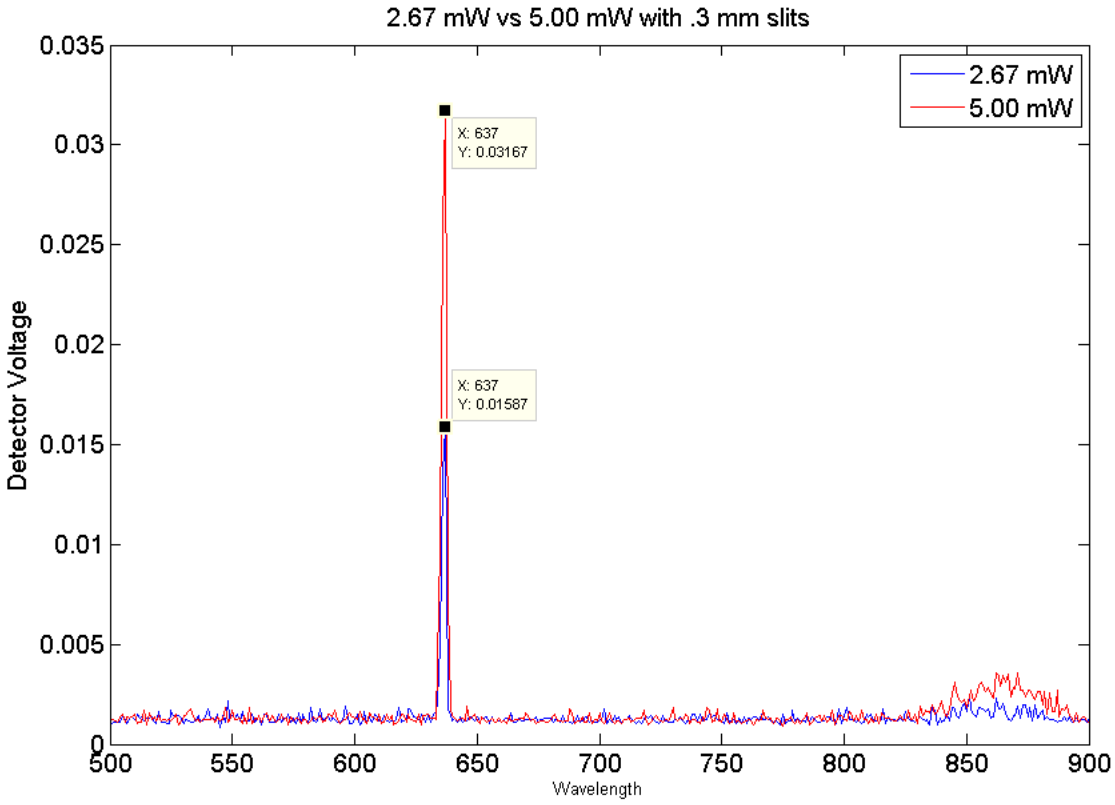

Figure 8: Graph of PL spectrum from GaAs with two different laser powers (2.67 mW and 5.00 mW), using .3 mm monochromator entrance and exit slits. The yellow boxes specify the wavelength and magnitude of clear peaks present.

Figure 8 shows the effect of laser power on PL spectrum when using the .3 mm slits (the smallest used for testing). The peak at around 637 nm is the laser peak. In theory this value should be at 633 nm, but due to issues with calibrating the monochromator that was used there is a slight deviation from this value. Note that the ratio of the laser peak intensities (in units of detector voltage) is (.03167V)/(.01587V) = 1.996. In theory this ratio should remain constant for all slit sizes, but we will see shortly that this is not the case. Interestingly, this is significantly different from the ratio of the laser power level used, which was (5.00mW)/(2.67 mW) = 1.873. Given that the detector voltage is proportional to the incident intensity as expressed in equation (1), the ratio of the laser reflection off of the sample for these two laser powers should be close to the ratio of laser power. However, the laser power was measured directly after the neutral density filter, and therefore does not take into account any losses from the optical chopper, mirrors, or other optical elements. It may be that these elements do not reduce laser intensity in a linear manner with increasing input power. Here the noise level is constant at an average of approximately .0011 Volts. The much weaker peak, broader peak around 860 nm is the PL emission from GaAs. Because of the small slit size, the signal to noise ratio on the PL signal is poor, and it is unclear where the peak of the emission is, especially for the 2.67 mW laser power setting; in this case the peak is barely distinguishable from the noise. In this case, even though the small slits will result in the best spectral resolution, the low signal to noise ratio results in data that is not of much use.

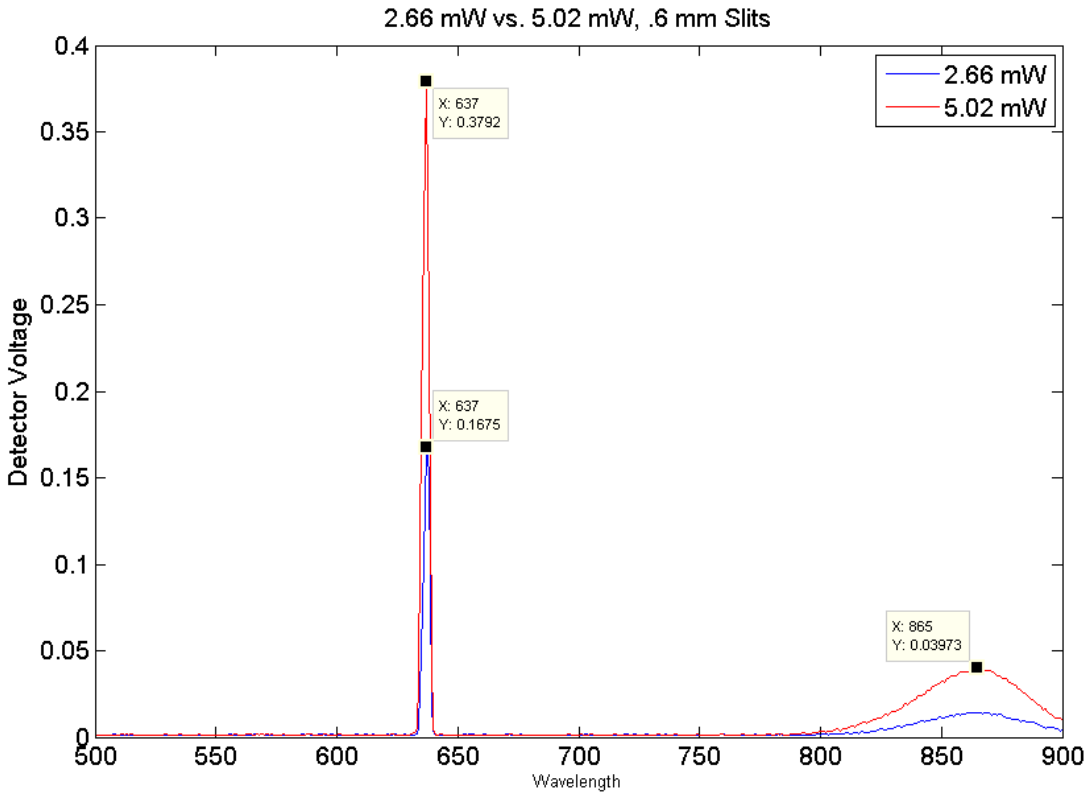

Figure 9: Graph of PL spectrum using .6 mm entrance and exit slits, showing laser peak (left) and PL emission peak (right). The PL peak at 2.66 mW is at 865 nm, with a magnitude of .01405 Volts. The other relevant peaks are specified in the yellow boxes. The noise level is once again approximately .0011 V. Note that Y axis scale here goes to .4V, while in the previous graph it was much lower at only .035 V.

The .6 mm slits produce noticeably different results than the .3 mm slits. The laser peaks are still clearly defined, and the ratio of their intensity is equal to approximately 2.266. Interestingly this is an even larger deviation from the ratio of laser output power, which is here equal to 1.887. The PL peaks are much more clearly defined, and now can be seen to have a clear peak at approximately 865 nm, which is very close to the accepted value of 867 nm. The signal to noise ratio for the 5.00 mW peak with this slit width is (0.03973V)/(0.0011V) = 36.11, while for the 2.67 mW power it is 12.77. Clearly the 5.00 mW power produces better results here, providing it is not of sufficient intensity to damage the sample. The laser peak voltages are approximately 10 times higher than with the .3 mm slits at both power levels.

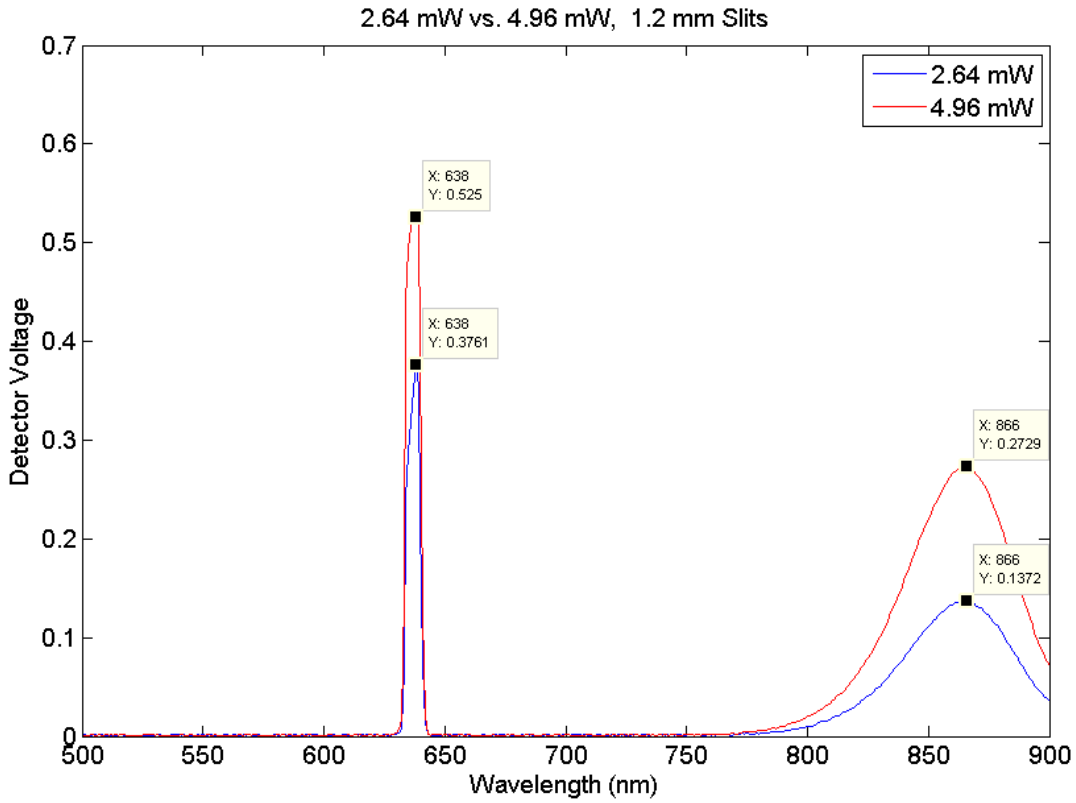

Figure 10: Graph of PL spectrum using 1.2 mm slits, with peak locations and intensities shown. Noise level is again approximately .0011 V.

The 1.2 mm slits show a much different picture with regards to relative peak heights. Here we see that the higher power laser peak is clearly not anywhere near 2 times the intensity of the lower power peak, but rather only 140% of it. This is due to saturation of the photoreceiver, which occurs at .5 volts with the gain settings that were used for these tests. The ratio of PL peaks here is 1.989, while the signal to noise ratio of the larger PL peak is 248, and the smaller 124.7. These are a significant improvement over the results from using the .6 mm slits. However, the larger PL peak is at .27 volts, which is closer to the saturation point of the detector than is ideal, given that PL measurements often vary by a factor of two or more (as will be seen in the microPL results). Both curves have a sufficiently high signal to noise ratio to give a well-defined peak, and in both cases it is 866 nm. The laser peaks appear to have shifted here by 1 nm, and are

slightly skewed to the right. It is possible that this is from saturation of the detector, although it may just be due to the fact that the wavelength steps are a significant fraction of the laser peak width, which can cause issues when the true maximum would lie partway between two wavelength steps.

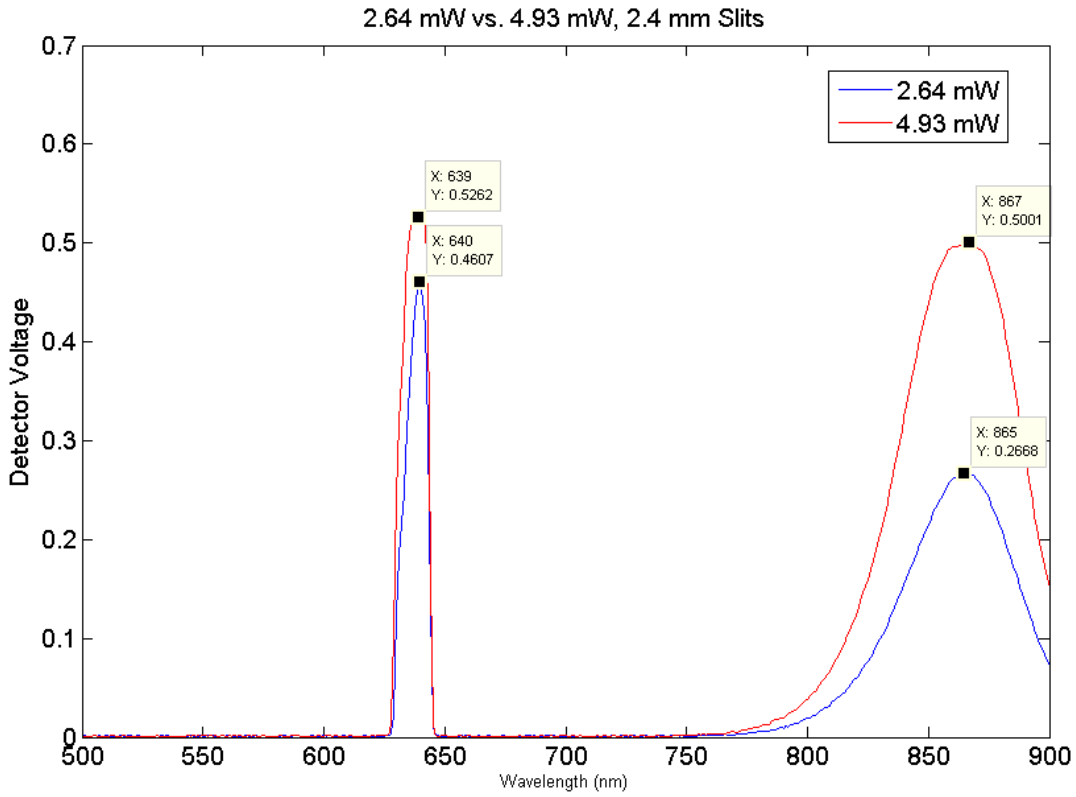

Figure 11: Graph of PL spectrum using the 2.4 mm slits. Noise level is still at .0011 V.

With the largest slits, the detector is being saturated by all peaks except the 2.64 mW PL peak. We see the tops of the laser peaks and 4.93 mW PL peak flattened significantly because of clipping in the detector. The signal to noise ratio for the peak that is not clipping is 242.5, which is comparable to the signal to noise ratio of the peak when using the 1.2 mm slits at 4.96 mW. However, using these larger 2.4 mm slits will give less spectral resolution, resulting in less accuracy for the peak location. The peak location itself should stay approximately the same, because although the large slit has less spectral resolution, it can be viewed as measuring a known quantity (the peak location) multiple times with an uncertainty equal to the spectral resolution. In this case, the PL peak distribution seems to be essentially symmetrical, so the

measured peak should be close to the actual peak. However, the lack of spectral resolution means that any smaller sub-peaks that would have been present may not be visible. For this reason, using the smallest slit that will provide a high signal to noise ratio will yield the best results.

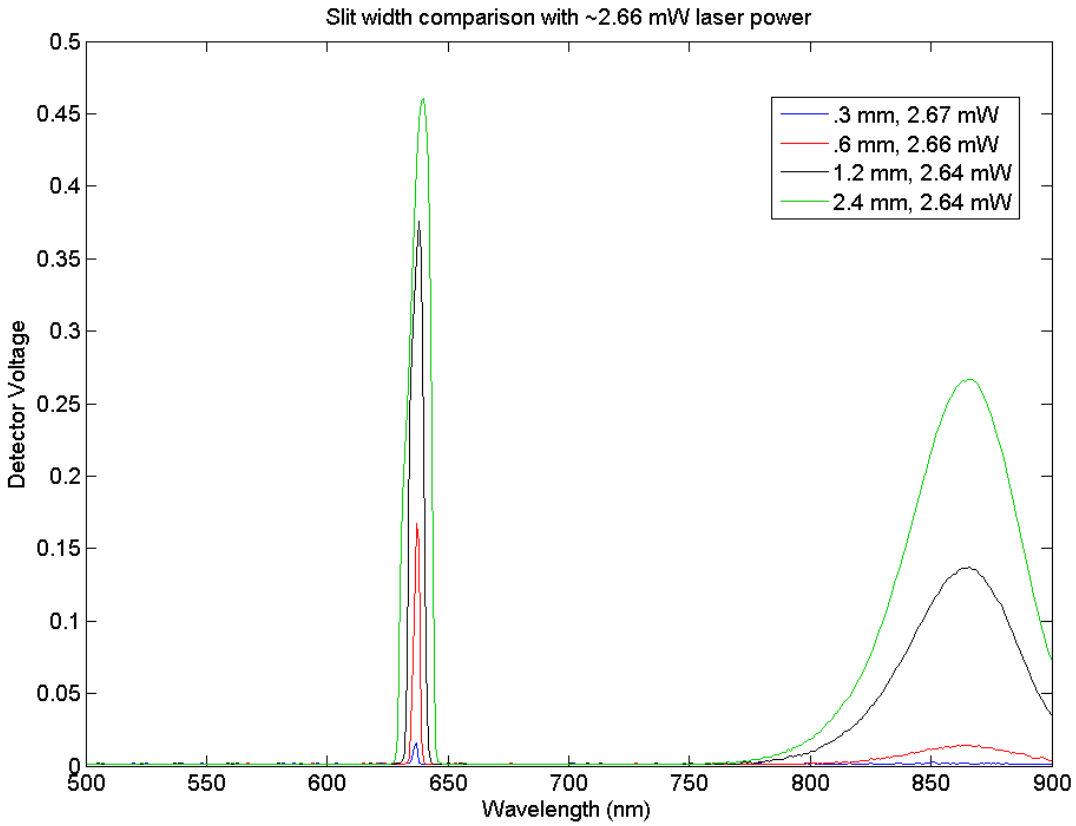

Figure 12: Graph of PL spectra with a laser power of ~2.66 mW using different sized entrance and exit monochromator slits.

Figure 12 compared the results of the tests using a laser power of approximately 2.66 mW, using the four different slit sizes. Here we can see how the different slit widths widen the laser peak varying amounts. This can be used to determine the approximate spectral resolution for each slit size. Wider slits let more of the spectrum pass through to the detector, and therefore the detector will be illuminated when the monochromator is tuned to wavelengths slightly above or below the laser peak. A typical HeNe laser has a bandwidth of approximately 1.5 Ghz at the

laser peak, which corresponds to a wavelength range of approximately 2 picometers[15]. Because of this we can essentially view the HeNe laser as a monochromatic source. This spread can be used to determine the wavelength range that the monochromator lets pass when it is set to a single wavelength.

In order to determine this spectral resolution, the full width at half maximum of each of the 4 laser peaks was calculated, shown in Figure 13.

Slit Width	Peak Width
0.3 mm	2.3 nm
0.6 mm	2.9 nm
1.2 mm	6.5 nm
2.4 mm	11.0 nm

Figure 13: Experimentally measured width of HeNe peak (FWHM)

This resolution determines what peaks can be resolved by the system. For example, when using the 2.4 mm slits, any peaks that are separated by 11 nm or less will not be clearly distinguishable. This fundamental tradeoff between intensity and resolution is a limit of the monochromator system used.

Figure 12 also allows us to better judge the effect of slit width on the PL peak itself. Because the PL emission peak for this sample is very wide, the slit width has a minimal effect on the measured peak width. The FWHM for the peak with the 2.4 mm slits is 54.3 nm, while for the 1.2 mm and 0.6 mm peaks it is 53.5 nm and 53.4 nm, respectively. The 0.3 mm peak is too noisy to determine an accurate width. The peak for all 3 of these tests is between 865 and 866 nm, which shows that, for broad peaks, the slit width does not have a significant effect on the measured maximum. However, as mentioned previously any smaller peaks within the range of the maximum that had been present cannot be resolved. In order to look at peaks caused by defect states at the band edge, high spectral resolution is required, as is lower temperatures than those used for this testing. At room temperature, these defect states in semiconductors are often full ionized at room temperature, and are not visible in the PL spectrum[16]. At low temperatures

the carriers are trapped at these states, so radiative recombination can occur, giving PL emission at the corresponding energy[3].

2. Spatially Resolved Photoluminescence (micro-photoluminescence)

In order to determine the spatial resolution of the system, linear tests were conducted on the fabricated sample. These linear tests scan along the horizontal direction, while keeping the vertical position on the sample constant. This allows a good idea of the linear resolution of the system when using the line features that were deposited on the sample. Chronologically, this sample was tested after testing another GaAs sample. The first sample that was tested (which will be discussed later) had much lower emission intensity. The test sample emission is much higher; even with 1.2 mm slits and 9.74 mW laser power, the peak intensity approaches the saturation point of the detector towards the end of the run, as shown in Figure 14. The testing settings used for this test are the same as those described for the standard PL testing.

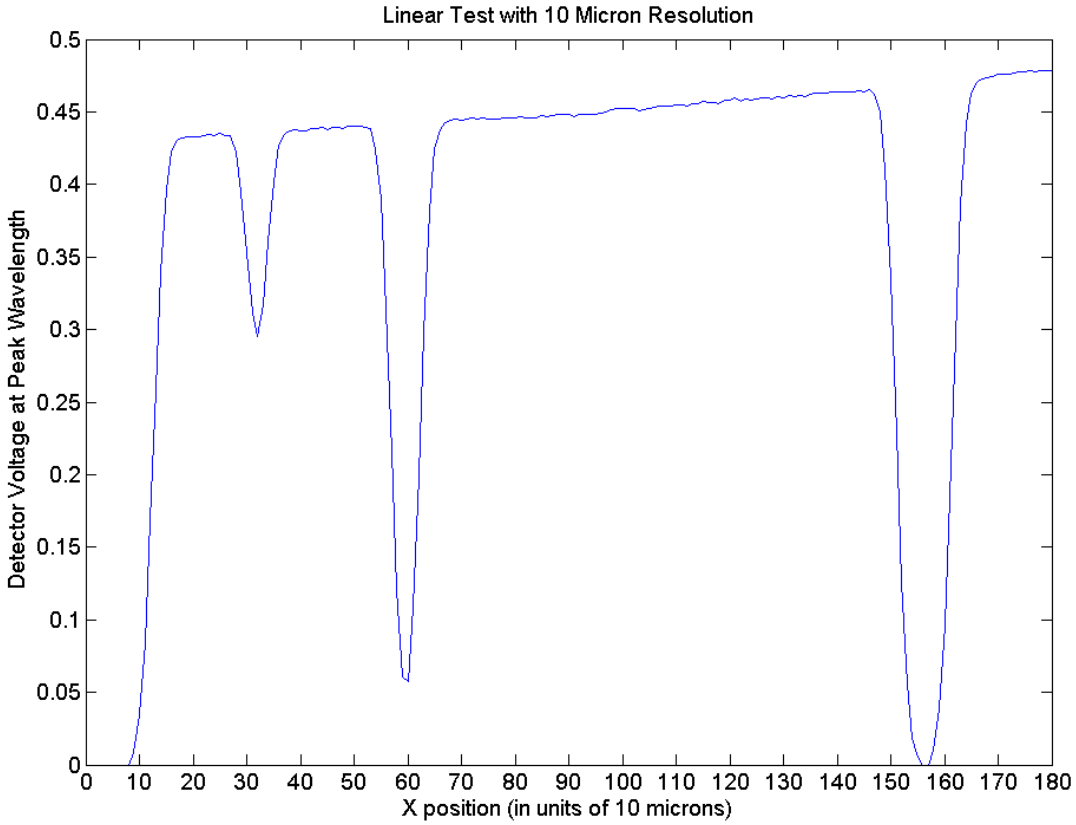

Figure 14: This data is from a linear scan across the surface of the test sample. The value at each position on the X axis is the amplitude detector voltage at the photoluminescence peak at that location. Because detector voltage and incident intensity are related by equation (1), this voltage is proportional to PL intensity.

In this plot, the first three chrome lines deposited on the sample result in a decrease in PL intensity in the surrounding area. Here, an amplitude of zero volts means that the detected peak was below .004 volts. However, as the noise level for these tests is typically at .001-.002 volts, a zero value here does not necessarily mean that there is no detected PL emission, but rather that there is very little. Peaks of such low amplitude are very noisy and ill defined, as seen in Figure 8. Figure 15 shows the actual surface of the sample in the region that was tested.

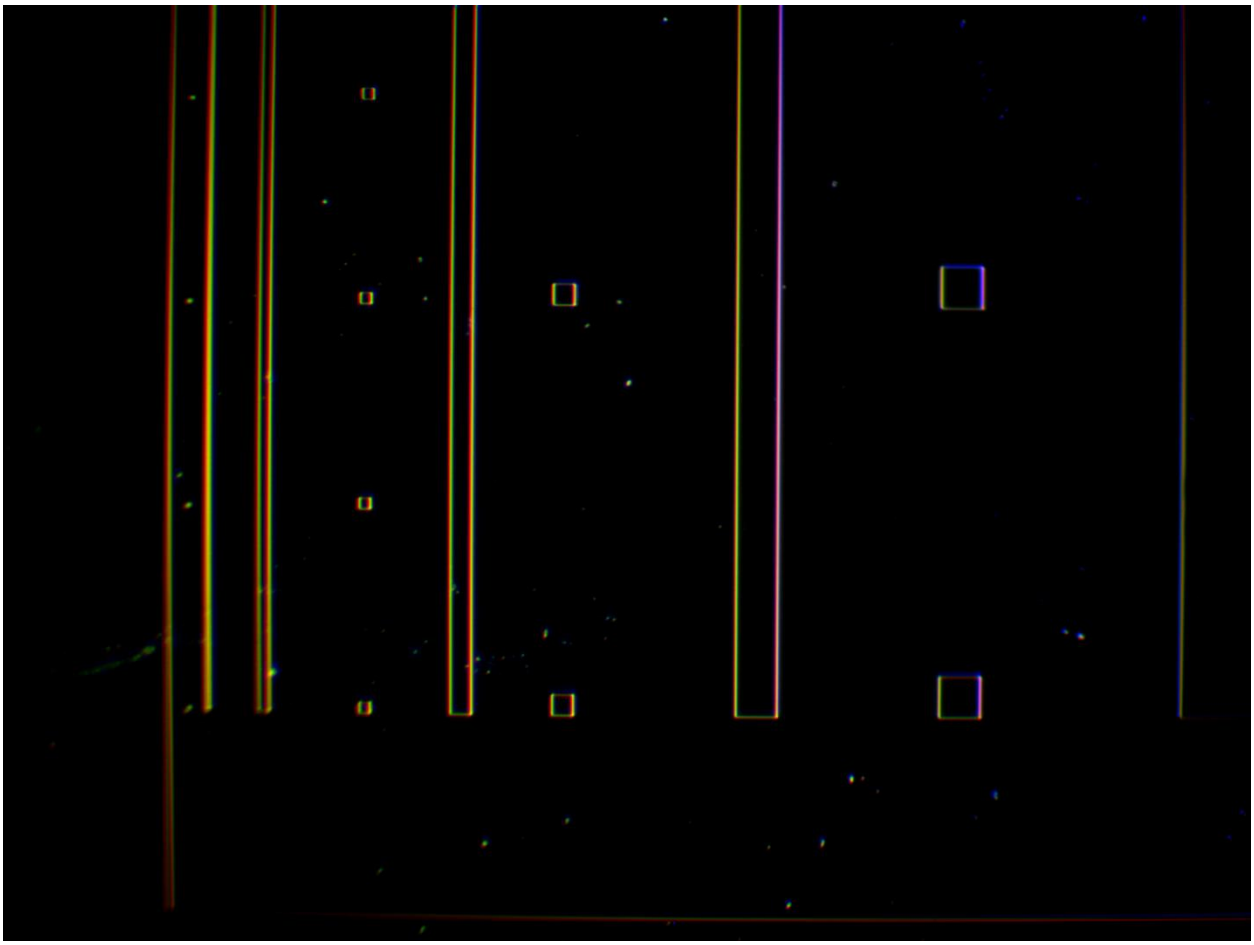

Figure 15: Color photo of test sample, zoomed in on area that was tested. The area to the far left of the sample is chrome, and therefore blocks all emission. Next are the 10 micron squares and 10 micron line, followed by the 50 micron line and squares, the 100 micron line and squares, and the 200 micron line and squares.

When this image is referenced, we see that the visible decreases in PL emission in Figure 14 are due to the first 3 lines on this sample. The testing was intentionally started at a horizontal coordinate that did not intersect any of the squares, to limit the results to linear resolution. The zero emission area on the far left of the graph marks the edge of the sample, which is surrounded by chrome. 100 microns in (10 units on the X axis), emission is detected and rapidly increases in magnitude as more of the laser spot is on the exposed semiconductor of the sample. The first dip in intensity corresponds with the 10 micron wide line. Because the laser spot is larger than this line, the intensity never reaches zero as part of the focused spot is always incident on the surrounding exposed GaAs in the region. The next dip in emission is from the 50 micron line, and produces a more significant decrease in intensity because a larger portion of the laser beam is blocked by the chrome. The final decrease is from the 100 micron line. The minimum intensity

in this region extends all the way to zero, which denotes that the peak intensity there was below .004 V. This suggests that when the laser is centered on the 100 micron wide line, there is very close to zero emission. This means that the majority of the laser power is focused on an area that is 100 microns in diameter, giving us an estimate of the practical spot size.

We can also estimate the spot size by seeing how much wider than expected these troughs are. If the laser had been focused to a spot of 10 microns in diameter or smaller, the 10 micron line would be exactly 1 unit wide, assuming the sample was lined up so that the spot was focused in the center of the line. However, we can see that this clearly is not the case, indicating that the spot is much larger than 10 microns. This results in a "blurring" effect, whereby the intensity gradually decreases until it reaches its minimum value when it is directly over the chrome coated feature. This decrease in intensity starts when the edge of the laser spot starts passing over the chrome coated area. If we assume that the PL emission intensity in this small region should be more or less constant, then this decrease in intensity occurs because a smaller portion of the laser is striking GaAs that is capable of giving off PL emission. Therefore, the left edge of this trough will occur when the right edge of the laser spot (when scanning left to right) has started passing over the chrome, and will end when the left edge has passed back onto the exposed GaAs surface after leaving the right edge of the chrome feature. Therefore, if we take this trough width and subtract the width of the chrome feature, we will get a reasonable estimate on the practical spot size.

For the 10 micron line, the trough seems to start at approximately 270 microns on the X axis (27 units from the left), and ends at 370 microns. This suggests a spot width of 90 microns. For the 50 micron line, the lower and upper bounds appear to be 530 and 670 microns. Subtracting the 50 micron width yields an estimate of 90 microns. For the 100 micron line, the bounds are closest to 1460 microns and 1660 microns, which yields a spot width of 100 microns. Here, the starting and ending bounds were taken as the values where the slope of the curve first starts steepening past +/- 45 degrees. A spot size of approximately 90-100 microns is further supported by the previously stated observation that the 100 micron line results in a lack of PL emission when the laser is centered on this feature. Interestingly, this spot size is smaller than the estimate of 172.5 microns calculated in section II. That estimate was based solely on the focal length of the lens and the beam divergence, which were both taken from manufacturer stated values; it could be that there is a deviation in these values that allows the spot size to be more

focused. Additionally, a Gaussian beam profile contains most of its intensity in the center; this means that the outer edges of the beam are much less intense and may not be capable of producing PL emission that is above the noise level.

These results indicate that linear defects that are 10 microns wide can be detected by the system. However, a line of 10 micron width will block much more of the laser spot than a square that is 10 microns on a side. Therefore, a 2D scan of the test sample was conducted to determine if spatially localized areas with no PL emission on the order of 10 microns can also be detected.

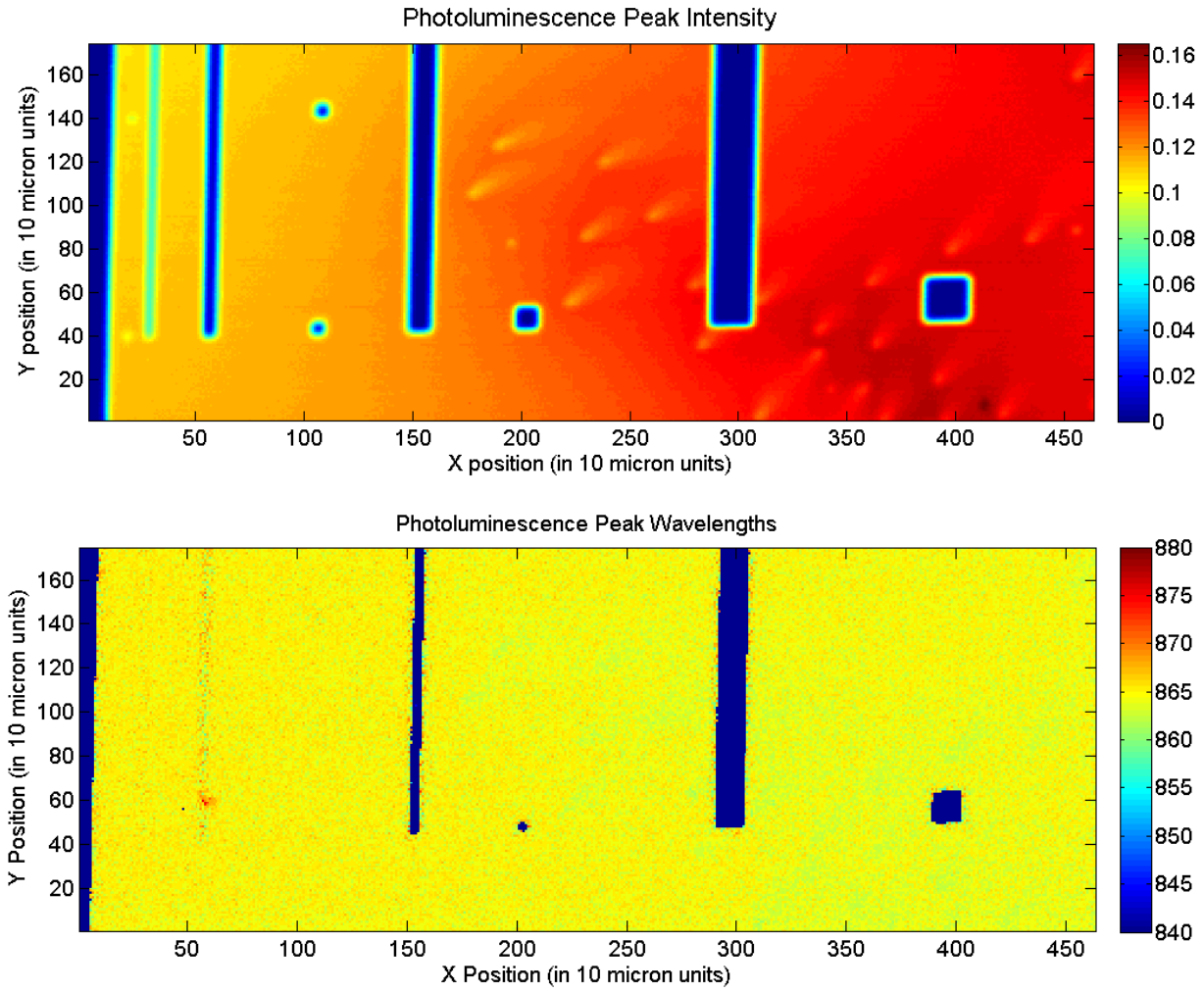

Figure 16: The PL emission peak intensity is shown, with 10 micron spatial steps (top). The corresponding wavelength of each peak is shown, with a zero nm peak corresponding to areas that did not contain emission above threshold (bottom). In the top image the color map scale to the right is peak voltage, while in the lower image it is peak wavelength. (in nm)

Figure 16 shows the results of this scan. This 463 x 174 resolution image was assembled by plotting the intensity of the PL peak data. This image contains 80,562 "pixels," each of which

represents a separate PL test. The total time for this test from start to finish was 78,786 seconds, or under one second per location, on average. This is significant, as early PL testing that I had done required much longer to obtain PL spectra of sufficient intensity (sometimes as long as a minute per location in very early tests). Even so, this time corresponds to 21.885 hours, which is a significant amount of time for an imaging procedure. Many more advanced PL systems utilize CCD cameras for detection, and illuminate the entire sample at once with an expanded laser beam. However, these systems typically only provide resolution on the order of a few hundred microns, and do not have the flexibility of wavelength range that this modular system has[17][2]. The two detectors available for this system allow it to be used from 300-1700 nm, and the cost is much lower than that of a CCD based system.

In the first section of Figure 16, we can identify not only all the linear features within the field of view, but also all of the squares as well. The 10 micron squares result in a slight increase in intensity, but one that is noticeable nonetheless.

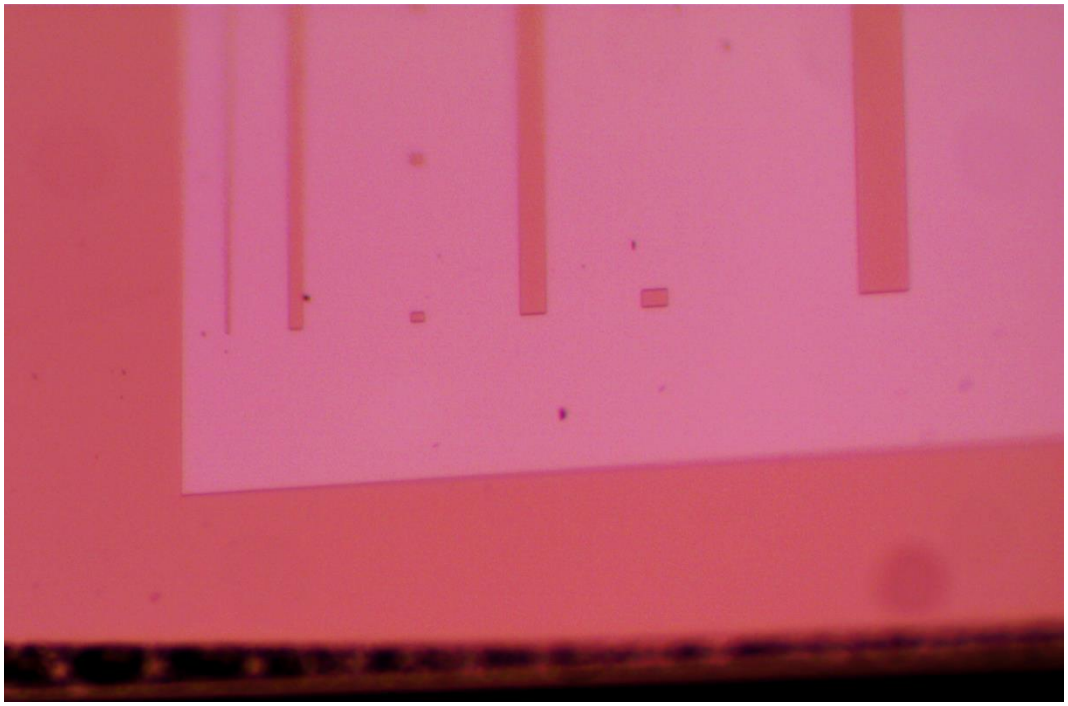

Figure 17: Photograph of testing area with diffuse light source specularly reflecting into camera

Figure 17 shows a close up microscope image taken of the testing area for reference, while Figure 18 shows the region containing the lower 10 micron square. Here we see that the 10

micron square does not result in as much of a decrease in intensity as the 10 micron line, but the decrease is nonetheless very much detectable.

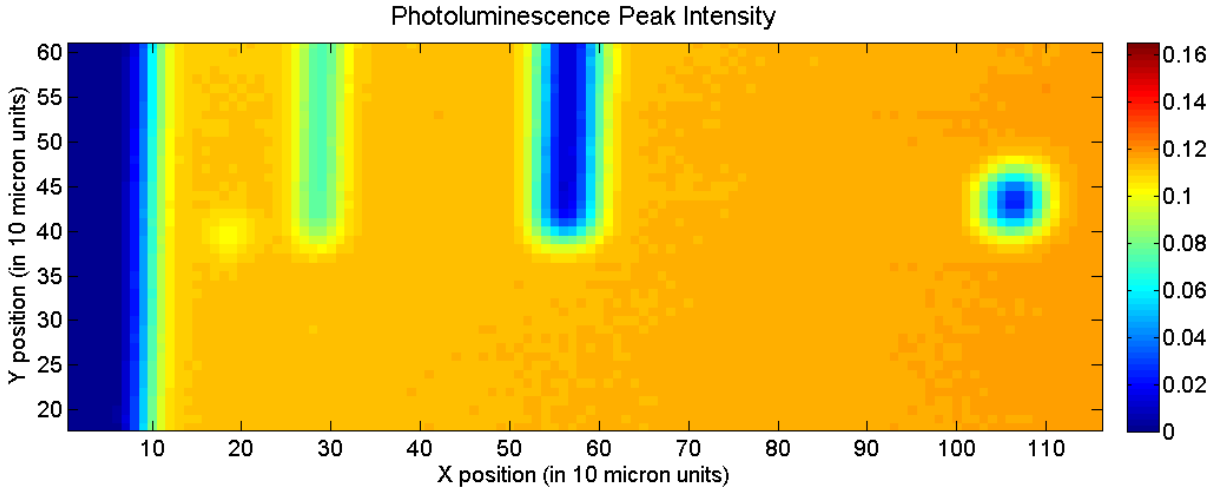

Figure 18: PL emission peak intensity image, zoomed in on region containing lower 10 micron square. Color map units are again in Volts.

The intensity of the peaks in the center of the 10 micron square is .10 volts, while the surrounding region averages about .11 volts. This is a small variation, but is clearly a significant one according to these results. The upper 10 micron square shows a similar difference, with an interior peak intensity of .097 V and a surrounding intensity of .107 V, again a .01V difference.

We see a general trend of increasing PL emission going from left to right over the sample, and a less severe increase in emission from the top of the sample region downwards. Since the "imaging" of the sample in this case took nearly a full day to complete, one might assert that this trend is due to changing environmental conditions, such as a temperature or humidity change. However, the raster scanning nature of the test setup allows for easy dismissal of such an occurrence. Because the sample is first scanned all the way across in the X direction before advancing in the Y direction, any variation of intensity that progresses in the X direction and extends through multiple lines in the Y direction cannot be the result of environmental changes, unless these changes are exactly periodic with the time it takes to complete one full scan line in the X direction. Similarly, while a variation in emission that is completely restricted to a single line along the X direction may be due to some environmental interference (such as

someone turning on the lights during a few detection steps), any feature that extends vertically through multiple Y values must be due to features on the sample, as imaging the region 1 unit above a certain X step occurs approximately 463 seconds later for this test (assuming 1 second per square), or nearly 8 minutes later. The chance of the same external interference occurring multiple times with this specific period is extremely low. In this way, the raster scanning method has an inherent self-validating ability for certain types of features. Since most features extend through more than one horizontal line, we can be assured that any such features are truly due to the sample.

The lower image in Figure 16 shows the wavelengths of the emission peaks for each PL scan. A zero value of wavelength is assigned to areas that do not have emission above threshold. The rest of the data at first appears mostly uniform, with values ranging between 864-866 nm, with what seems to be a distribution consistent with random variation due to noise. However, there is a small region very close to the 50 micron line at (X, Y) = (58, 59) that apparently has a peak wavelength of 875 nm, a significant deviation from the average. Because the testing code preserves all spectral data, we can look at the actual PL emission spectrum at this location, and compare it with the spectrum at (67, 58), which seems to be fairly representative of the region surrounding it.

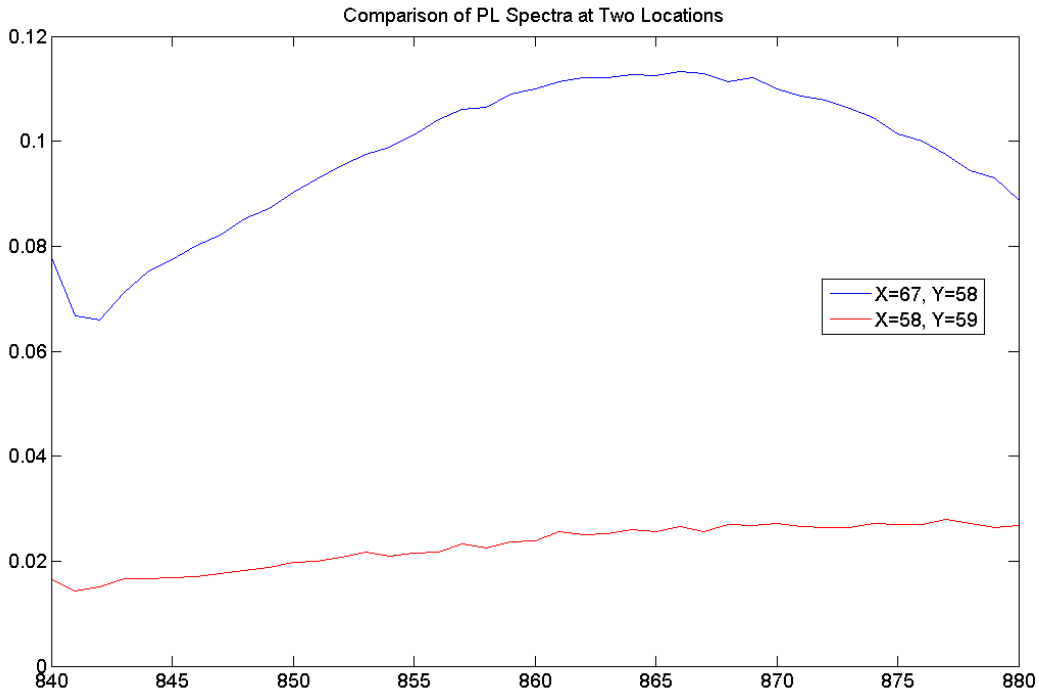

Figure 19: Comparison of emission spectra at two different locations on the sample, as given by their spatial coordinates.

We can see from this data that the 875 nm peak is much less defined than the "normal" 865 nm peak, and is of a much lower intensity as well. This is to be expected, as the coordinates (58, 59) appear to be nearly on top of the 50 micron wide chrome line. The ill-defined nature of this weaker peak suggests that the peak wavelength shift may not be significant, but rather an artifact of noise. We also see that there is what appears to be a secondary peak all the way to the left of these graphs at 840 nm. This is present at other locations in the test as well, and is likely due to a slight overlap in the timing of the system, where the monochromator is not completely done resetting from 880 nm to 840 nm before the measurement for the next location has started. This is not an issue for this data, since the expected peaks are far from the 840 nm starting point. Since the monochromator does not have a way to report when a move is completed, it cannot be timed in an exact manner like the movement system can (the XY stages can be queried for their current positions while moving, while the monochromator cannot). As discussed previously I had to use a 100 ms timer for the monochromator reset step in the code; this was apparently ever so slightly too short, and adding a few milliseconds to this timer would likely have fixed the issue. However, making this timer unnecessarily long can add a significant amount of time to the overall testing duration.

Some other interesting results become apparent when we rescale the colormap range for the peak wavelength image. This is shown in Figure 20.

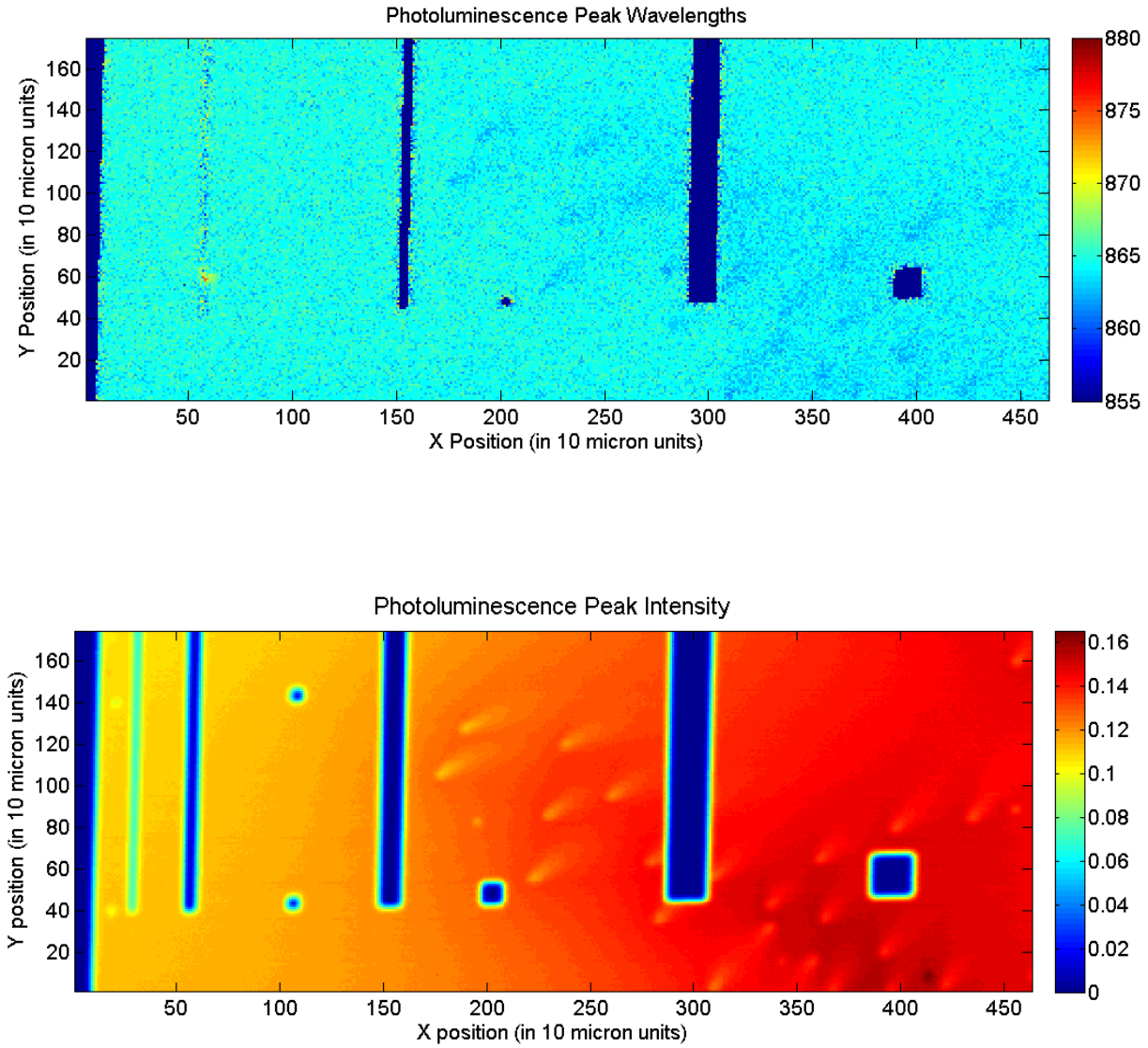

Figure 20: PL peak wavelengths, with color map scale range reduced to 855-880nm from the full scan range of 840-880 nm (top). The same image from the second part of Figure 16 showing the intensity is shown below for comparison.

By reducing the color map range, we can get better contrast to see small variations in PL wavelength that may significant. Since there are no PL peaks below 855 nm anyway, no data is lost by this range compression. Had there been any peaks below this value, they would be mapped to the lowest value of 855 nm, thereby clipping some of the data. In Figure 20 we can

see a number of regions of lower wavelength throughout the right side of the image (the darker blue concentrations mostly to the right of X=170) where the peaks are located at approximately 862 nm instead of the typical value of 864-866 nm. These regions coincide almost exactly with the "comet shaped" areas of lower intensity throughout the intensity colormap in the top image of Figure 16 (also shown here again for direct comparison). The fact that these wavelength shifts correspond to an experimentally significant decrease in intensity suggests that they are the result of variations in sample properties in those regions. This shorter emission wavelength corresponds to a slightly higher energy band gap. One possible explanation for this is variations of doping concentration; a higher doping concentration in an N type semiconductor will add more states just below the conduction band. With high enough concentrations there are enough states present to effectively shrink the band gap in what is known as band gap narrowing[18]. Therefore, the regions of lower emission wavelength may have lower dopant concentrations. This is supported by experimental tests that have been done on N-Type Germanium, another direct band gap semiconductor, which show that a higher dopant concentration results in not only narrowing of the band gap, but also higher PL intensity. Therefore, both the locally lower PL intensity and higher band gap energy support the hypothesis that these regions are due to lower dopant concentrations.

Before the microPL testing sample was fabricated, other 2D testing was carried out on another N-type GaAs sample with no intentional surface features as in the other sample. An image of this sample is shown in Figure 21 below.

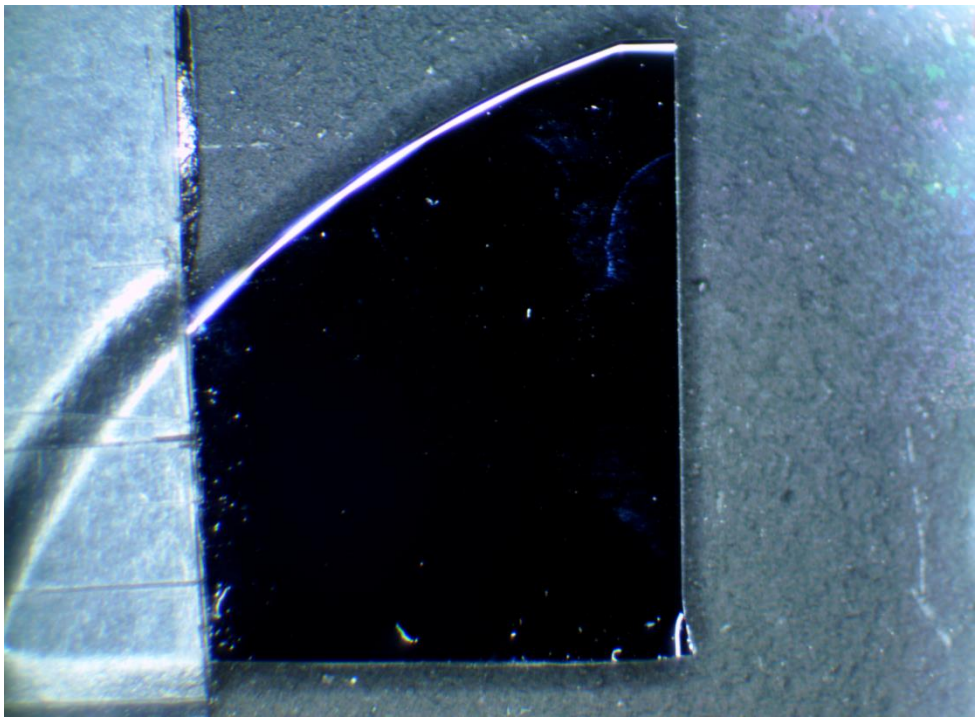

Figure 21: first GaAs microPL testing sample

This sample was primarily used for optimization of the code for the microPL system. Prior to conducting very high resolution tests, it was necessary to reduce the duration of the testing as much as possible by removing unnecessary steps and speeding up the actual PL measurements as much as possible without compromising the results. A number of linear tests were conducted on this sample with various step sizes, but were run more for testing purposes than to produce meaningful results, and therefore will not be discussed here.

The first 2D test carried out on this sample used 50 micron steps, and investigated a region in the middle area of the sample, away from the edges. As this was an early test, the region studied was small, with only 60 horizontal lines and 41 vertical lines. Because the emission intensity on this sample was in general much lower than the PL test sample, the full 22 mW laser power was used for all of these tests.

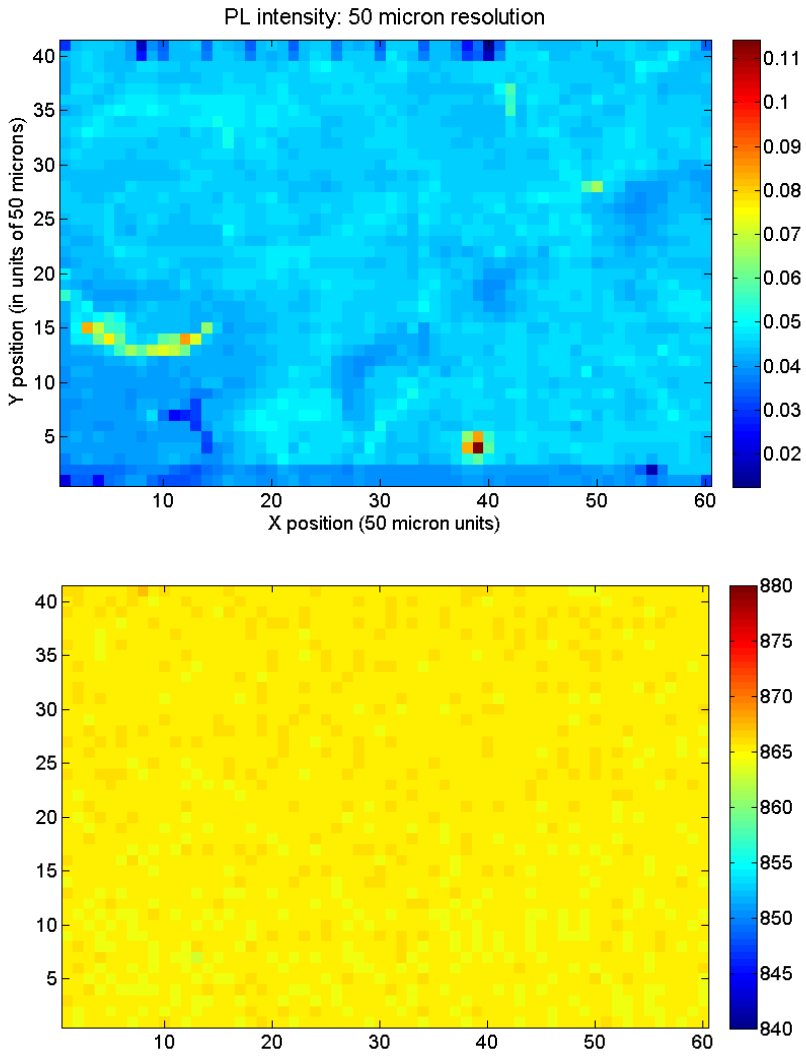

Figure 22: PL peak intensity scan at 50 micron resolution (top), PL peak wavelength scan of same sample (bottom)

Unlike with the previous sample, there are significant variations in PL intensity across this small region, and they are abrupt instead of gradual. The lower right corner has an area of higher emission with an area of lower emission immediately below it. The peak wavelengths, however, are essentially constant throughout the sample at about 865 nm. There is a slight trend towards shorter wavelength peaks at the bottom of the sample and longer wavelength peaks at the top of the sample.

The next area was scanned at a 25 micron resolution, as shown in Figure 23.

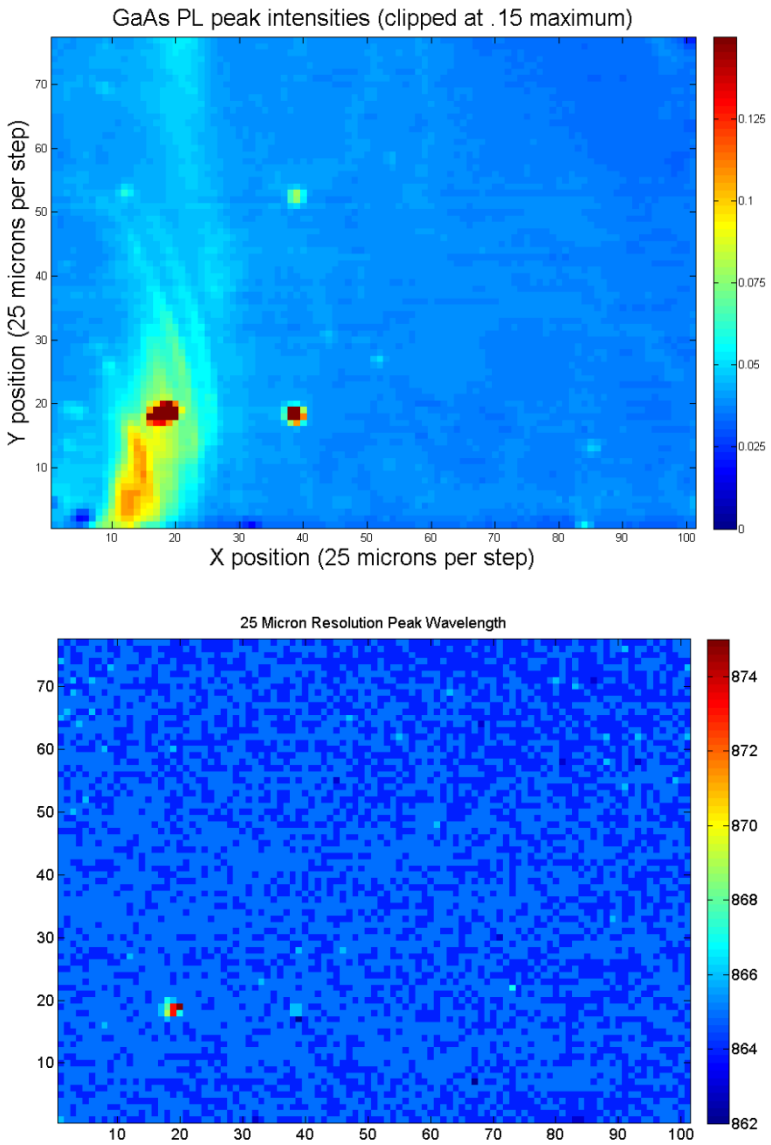

Figure 23: PL peak intensities at 25 micron resolution (top), PL peak wavelengths over same region (bottom)

The most notable feature of this region is the area of higher intensity in the lower left corner. Also present is a small region around (20, 20) that is of a much longer peak wavelength, and a much higher intensity. However, after cleaning the sample, this anomaly was no longer present in following scans, which leads me to believe it was simply a foreign contaminant that had some fluorescent emission (which is supported by the fact that the peak at that spot is not only of higher intensity, but is much wider as well). The data was clipped at .15 volts, as the actual emission intensity of this bright spot was significantly higher, going up past .2 volts at the detector, while the maximum for the rest of the region was much lower.

After performing these two smaller scans on the surface of the sample, a scan was performed on the entire region, with a resolution of 50 microns.

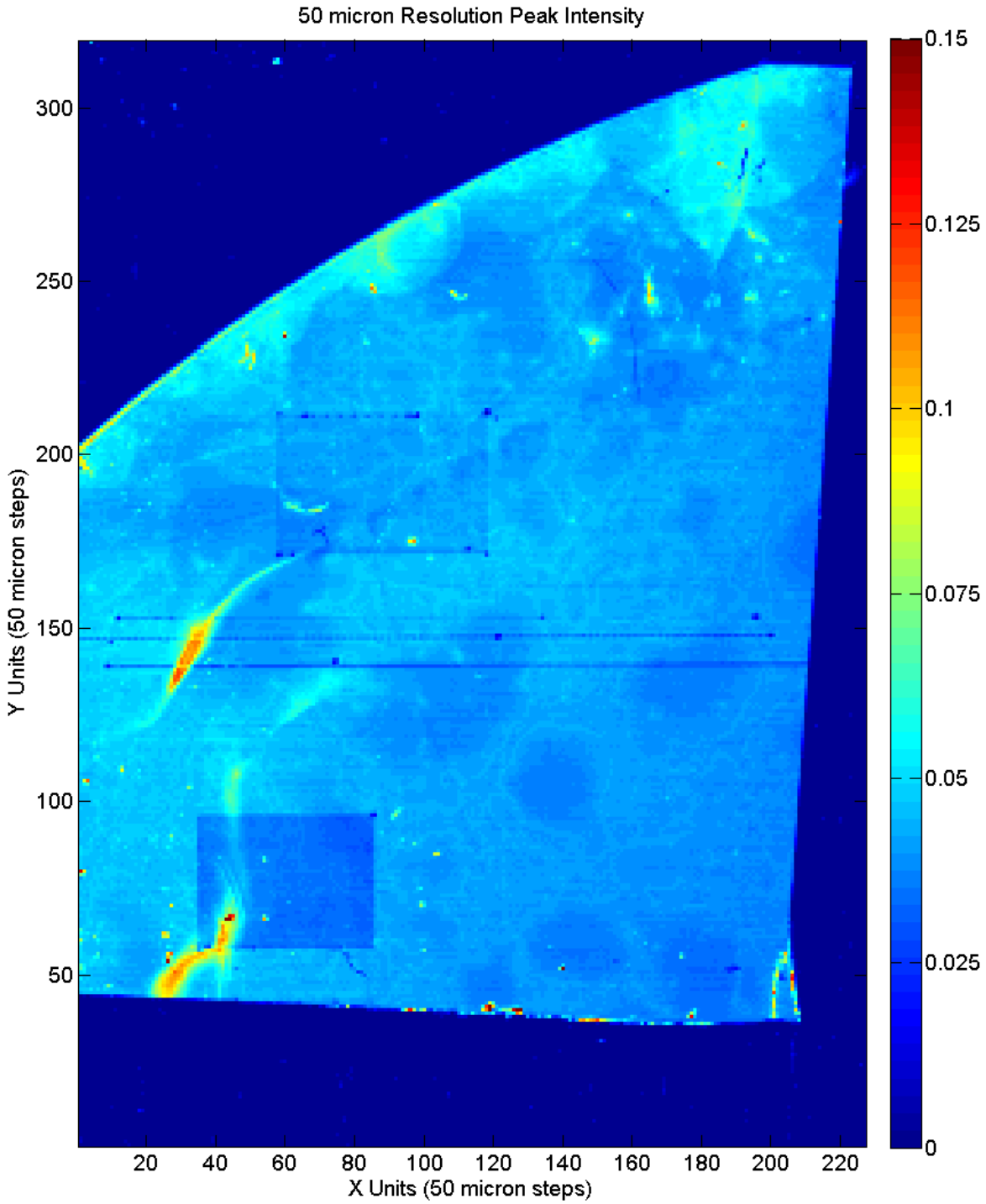

Figure 24: PL Intensity of entire sample with 50 micron steps. Data is again clipped at a maximum detector voltage of .15 V because of the much higher intensity spot on the sample.

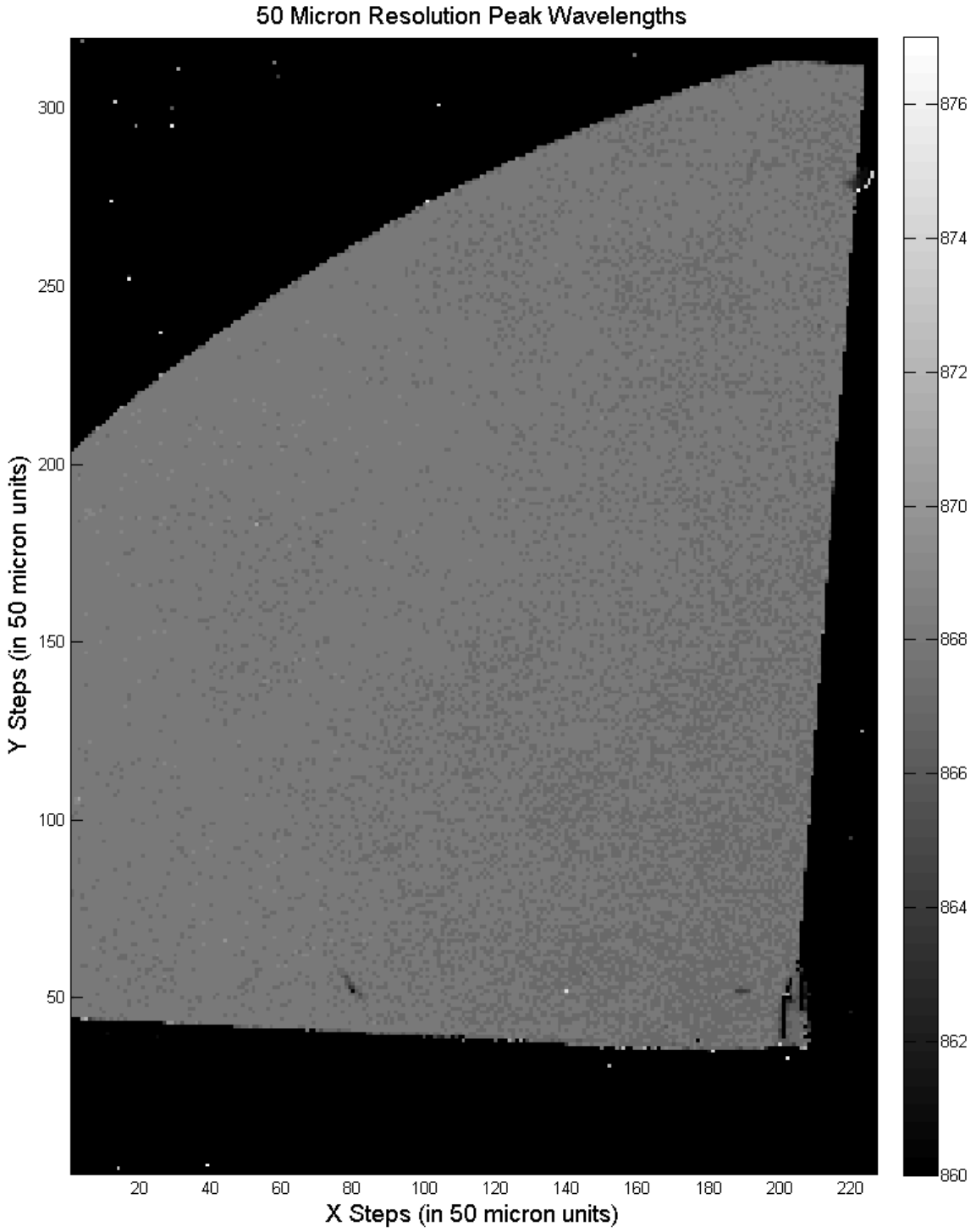

Figure 25: Emission Peak Wavelengths for the same sample. The scale here has been constrained to 860-876.5 nm from the full testing range of 840-880 nm because there are no areas on the sample itself with emission wavelengths outside this reduced range. A greyscale color map is used here for better visibility.

These scans show some interesting results. The intensity image shows some localized regions of around double the intensity of the bulk of the sample ((about .125 V vs the typical sample values of .05-.06V). However, the most notable properties are the dark regions on the sample. Towards the middle of the image we see dark lines, some of which appear to be solid, and others are a series of dark spots. There is also a square, darker region in the top left of the sample, and an even darker square on the bottom left of the sample. These darker areas are a result of prior testing on the sample. The lines are from the various linear tests that were conducted, with the "dotted" lines caused by lower resolution tests and the "solid" lines from higher resolution tests. As these lines pass through the higher intensity region near (20, 150), the intensity of that feature is reduced as well. The upper square is the same region that was scanned in Figure 22, while the lower square is the same area as Figure 23. These darker areas appear to be from some sort of laser induced damage to the sample that reduces intensity of the PL emission. The lower square region is darker because it was scanned at 25 micron resolution, which translates to a slower scan, and therefore each location on the sample is exposed to the laser for longer.

While this seems like an unfortunate consequence of the testing, it also serves to validate the operation of the system. This photobleaching-like process allows the locations of previous scans to be seen clearly. We can see from this image that the square regions scanned in the previous tests were in fact square as intended, and that observed areas of higher and lower emission are still present days later (these tests were conducted over the span of a few weeks). This reduction in intensity means that this testing has the capability to be at least partially destructive given high enough laser power. However, there was insufficient time to fully investigate what mechanism is causing this reduction in emission, and if it is truly irreversible damage or not.

Other than this laser damage, we can see much more variation across the surface of this sample when compared with the microPL test sample. The right side of the sample has overall less emission, with circular regions of even lower emission. The areas of moderate emission (a detector voltage of ~0.05 V) seem to be form an almost weblike structure around these areas of lower emission (voltage of ~0.03V). We also see the areas of much higher emission (regions of greater than 0.1V). There is also a region at approximately (80, 50) that appears to be a line of lower emission. On the PL peak wavelength graph, we see that this region corresponds to a

shorter wavelength peak as well (approximately 860 nm). Looking back at the actual image of the sample in Figure 21, we can see that this line corresponds to a visible mark on the surface of the sample.

As with the microPL test sample, the area general trend of lower emission towards the lower right hand side of the sample is accompanied by shorter emission wavelength in Figure 25. As before, this could potentially be caused by a lower concentration of dopants. The areas of high emission, however, do not seem to be correlated with significantly shorter band gap due to band gap narrowing, and therefore may not be due to high dopant concentrations.

In one final test on this sample, a final 25 micron resolution test was carried out on the lower part of the wafer, shown in Figure 26.

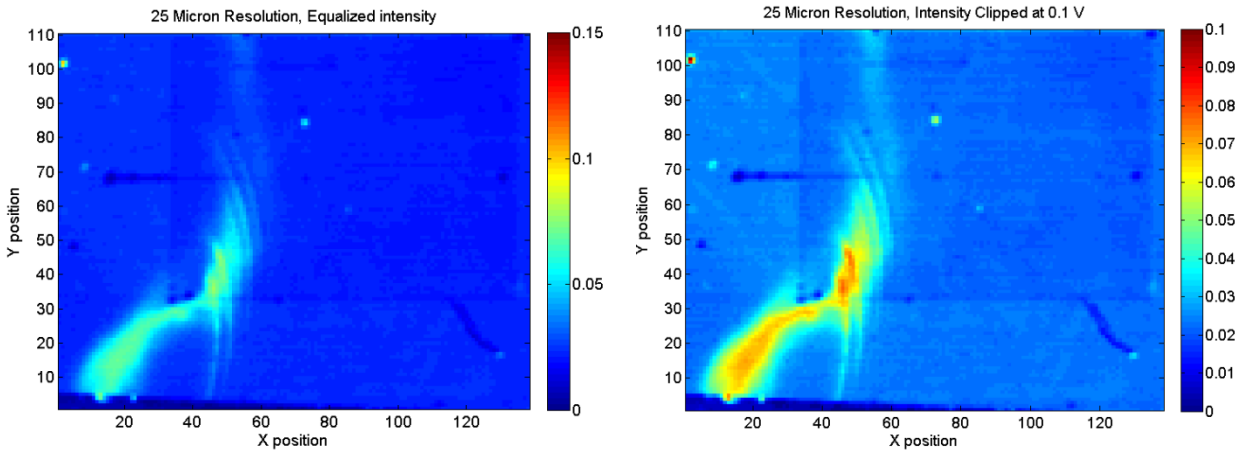

Figure 26: Final 25 micron resolution test of lower left region of sample, showing laser degradation. The left image has the same colormap scale as the image in Figure 23 (0-.15 volts), but appears much darker due to degradation from multiple scans of the region. The area of the previous scan can be seen as the even darker square in the upper right corner of the image (this scan scanned a slightly larger region). The right image shows the same data, but with the colormap scaled to a narrower region that better suits the data range (0-.1 volts).

These two images show the effects of the laser scanning the surface of the sample multiple times. Inset in these images we can see the square from the first test of the region. When the voltage scale is set to the same scale as used for this earlier scan, we see how much of a decrease in intensity each scan causes. However, when we rescale the voltages to better fit the data range, all of the intensity relationships are still intact, and nothing has been "washed out." The step size on these images is 25 microns instead of 50 microns, resulting in smoother edges on features, with less image aliasing. Additionally, the sample was cleaned with deionized water prior to taking these images, and the bright spot in the lower left corner is no longer present, supporting the assertion that it was a foreign contaminant.

For a final test, the anomalous area located on the microPL test sample was tested with 10 micron step sizes.

Figure 27: Image of anomalous area on microPL test sample

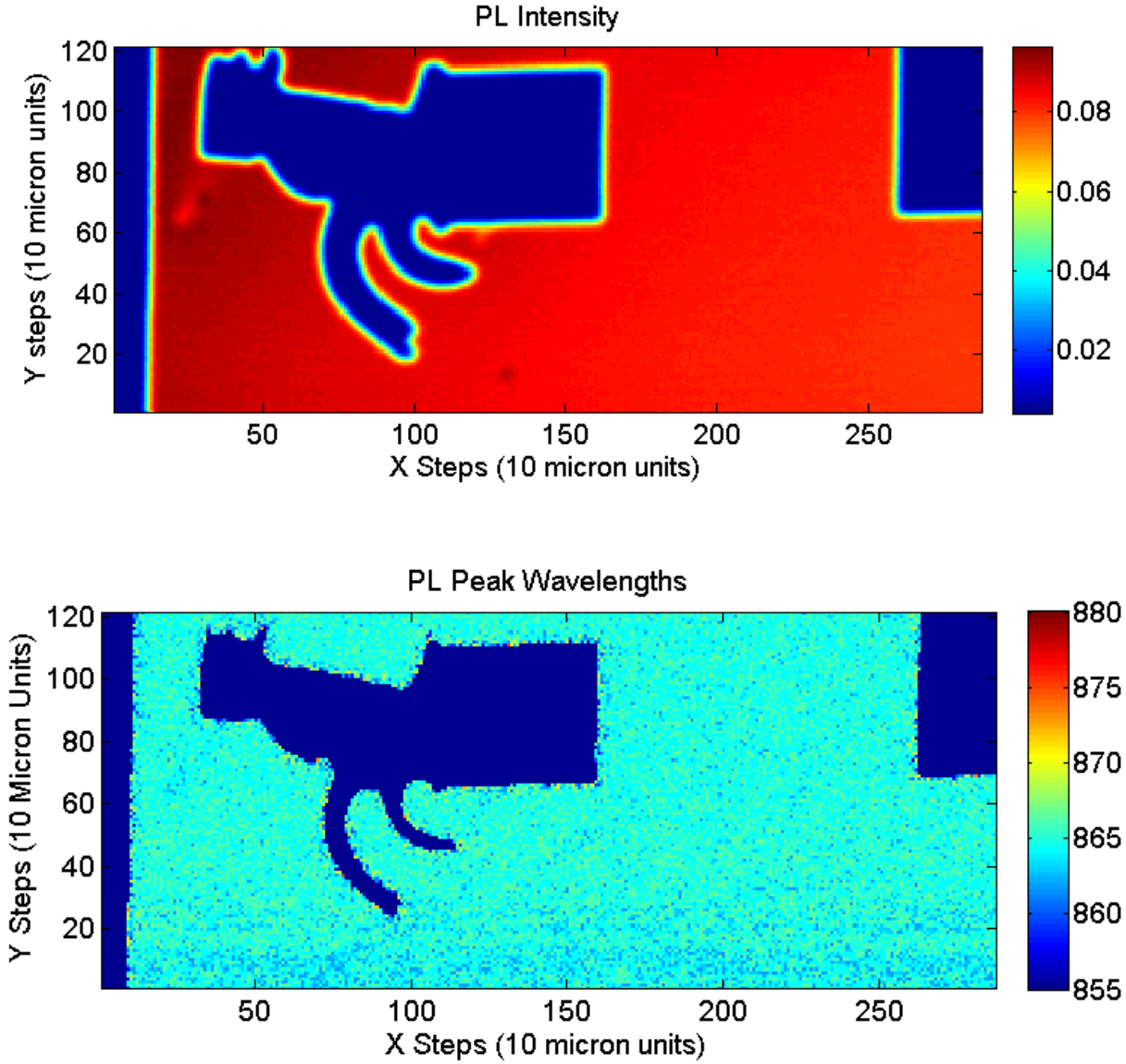

Figure 28: PL intensity (top) and wavelength (bottom) images for the region of the test sample containing the anomaly.

These tests give us a clear image of the artifact. It seems to be completely blocking PL, and is therefore most likely additional metal that was deposited on the surface due to problems with some stage of the photolithography or deposition process. This also shows how more complex shapes can be imaged using the system.

V. Conclusions and Future Work

Through the course of this research, a system was developed that could successfully detect certain features on the surface of semiconductors on the order of 10 microns using photoluminescence emission. This could potentially be used for characterization of these materials, such as defect location, or for determining how the properties of the semiconductors, such as doping concentration, vary throughout the semiconductor. The main operating parameters of this setup were determined theoretically or experimentally. However, there is much room for improvement with this system. The next logical step would be to continue optimization of the current system by reducing the laser spot size further using a beam expander or more powerful optics. Reducing the testing time significantly more for the microPL system is not possible with the current equipment due to the limited scanning speed of the monochromator. However, there are other devices such as CCD spectrometers that can bypass these restrictions by using a CCD to capture the diffracted spectrum instead of scanning through the wavelengths. These systems effectively view the spectrum all at once, allowing the system to get a spectrum in a matter of milliseconds. If a sufficiently sensitive CCD spectrometer could be found, it would speed up the process significantly (as the XY stage is capable of making micron sized movements fairly quickly).

The modularity of this setup also allows it to be converted to study different things. A cryostat could be used to cool the sample down using liquid nitrogen to obtain more information about defects using standard photoluminescence. The adaptability of the monochromator system allows it to study any wavelengths within the grating and detector range, allowing wider, more broadband scans to be done as well as more focused scans of narrower regions. Similarly, the microPL system can be used to first scan the surface of a sample with larger step sizes to reduce the testing duration, and then any areas of interest can be examined more closely at higher spatial resolution, or over a larger wavelength range.

One potential future investigation would be to determine what is causing the laser degradation on the samples, and see if this is reversible in any way either by annealing to attempt to reform any broken bonds, or cleaning the sample to remove any surface film that may be cause reduced emission. Since a main use of this setup is nondestructive characterization of materials that are going to be used to construct devices such as photovoltaics, any tests that

reduce emission and therefore solar cell performance are not ideal. Fortunately, at lower intensities (under 10 mW), the samples did not seem to be as susceptible to damage. The slit and power tests at the beginning of section IV were performed on the same location on the sample, and at those lower powers there did not appear to be a decrease in emission. However, that sample had much different behavior overall when compared with the other sample, so there may be many more factors at work.

Further validation of the setup could be achieved by testing a wider range of materials with varying band gaps. Although only one material was studied here, other semiconductor materials could easily be investigated provided their band gap is within the range of the detectors and monochromator, and lower in energy than the laser wavelength. Additionally, samples with known types and concentrations of defects could be imaged with the microPL system to determine the signature different defects yield, so that they can be detected in materials fabricated in the laboratory in the future.

Appendix

I. Standard PL Labview Code

Front Panel (user interface):

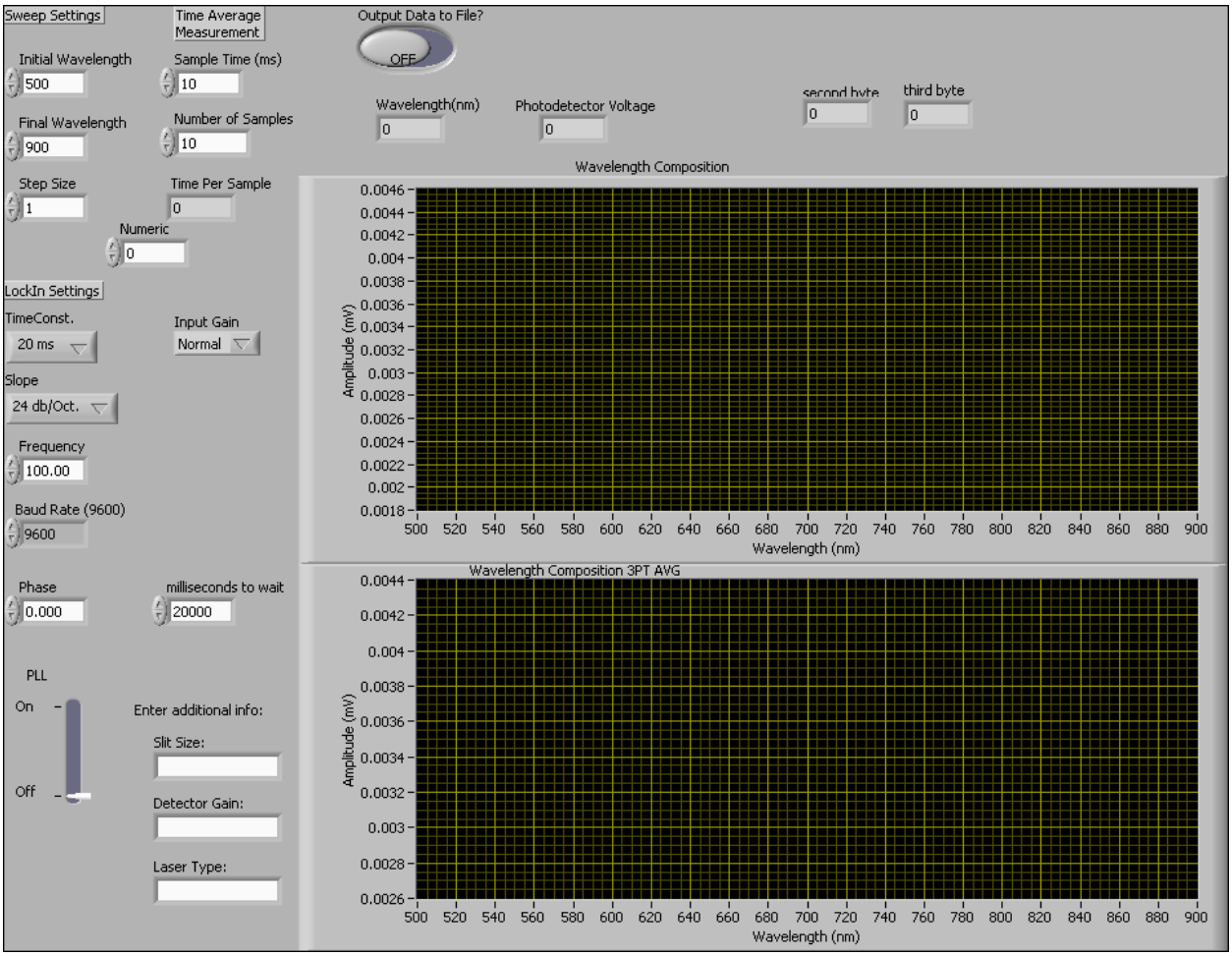

Block Diagram:

(Code goes from left to right on each page, and is split into 3 parts)

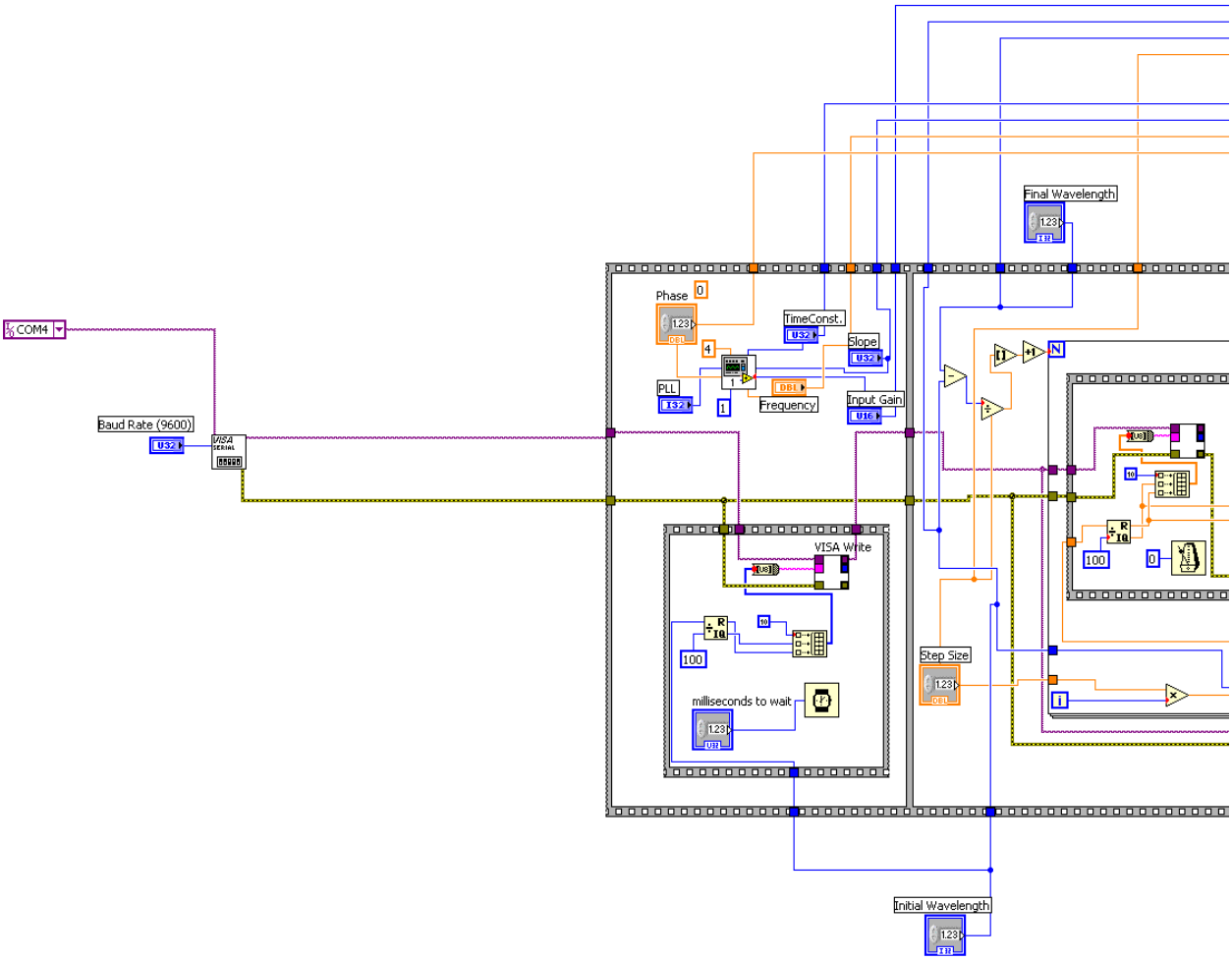

Block Diagram (part 2 of 3)

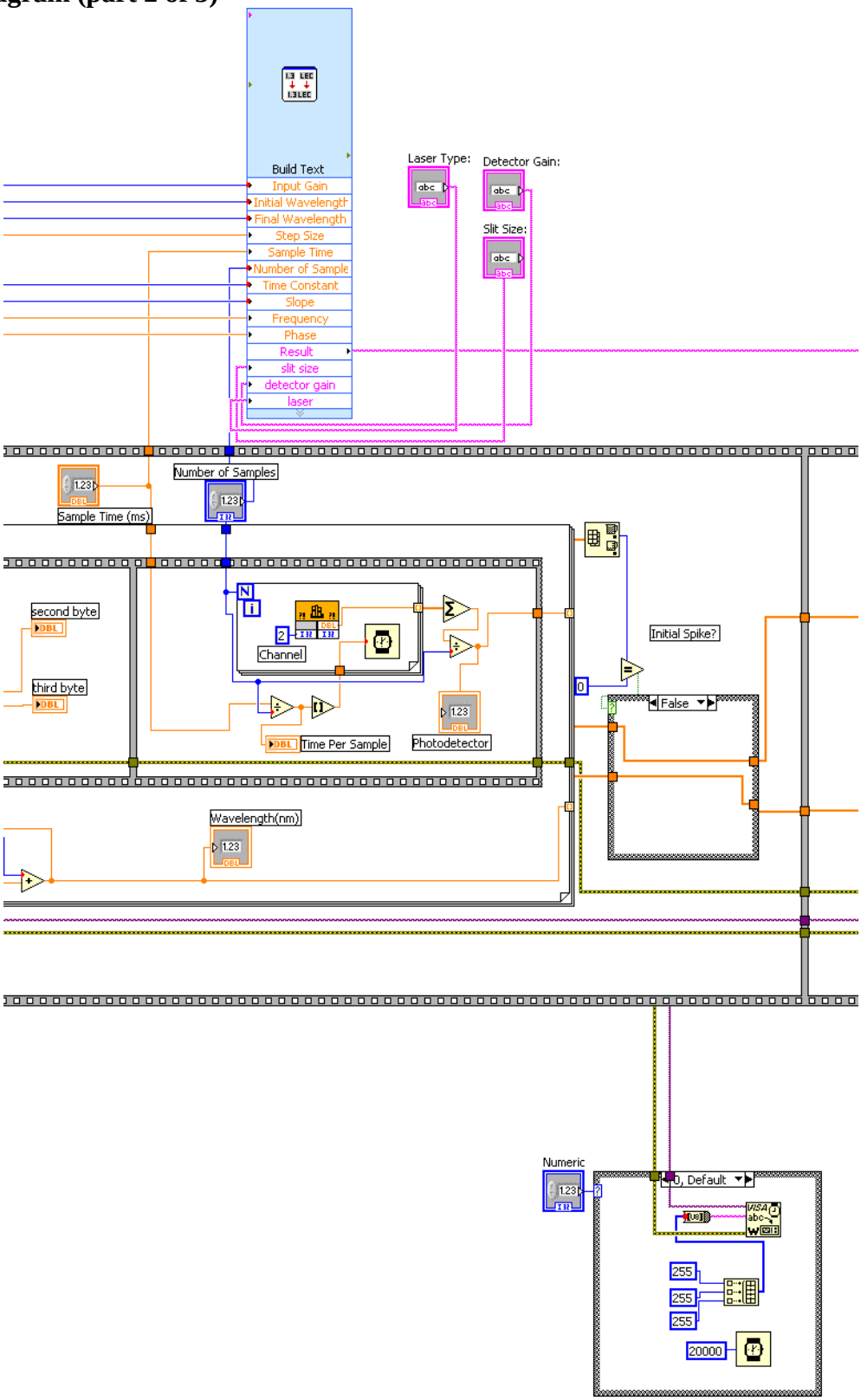

Block Diagram (part 3 of 3)

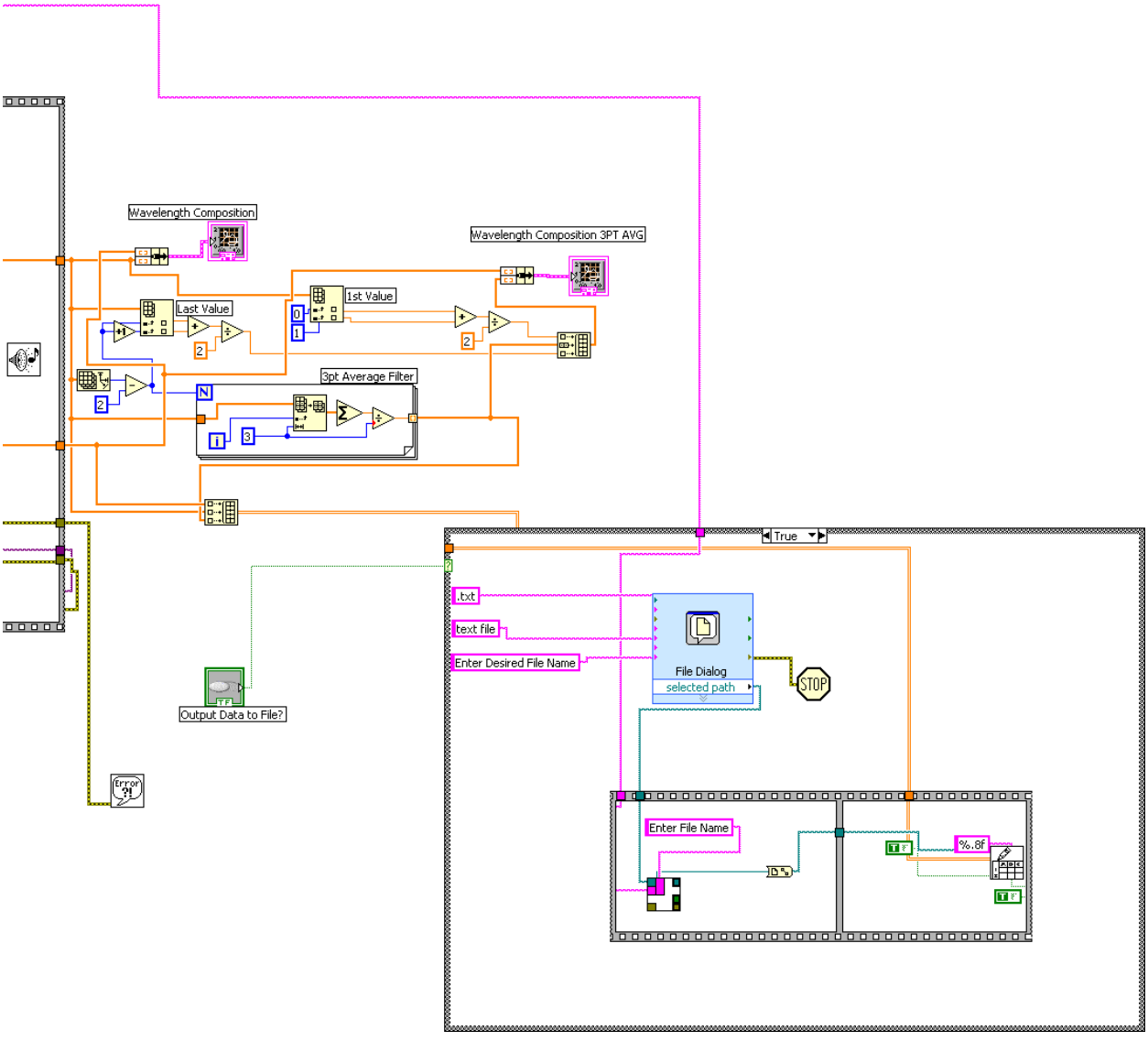

II. MicroPL Code

Code for reporting of XY stage location, showing front panel interface (top) and block diagram (bottom):

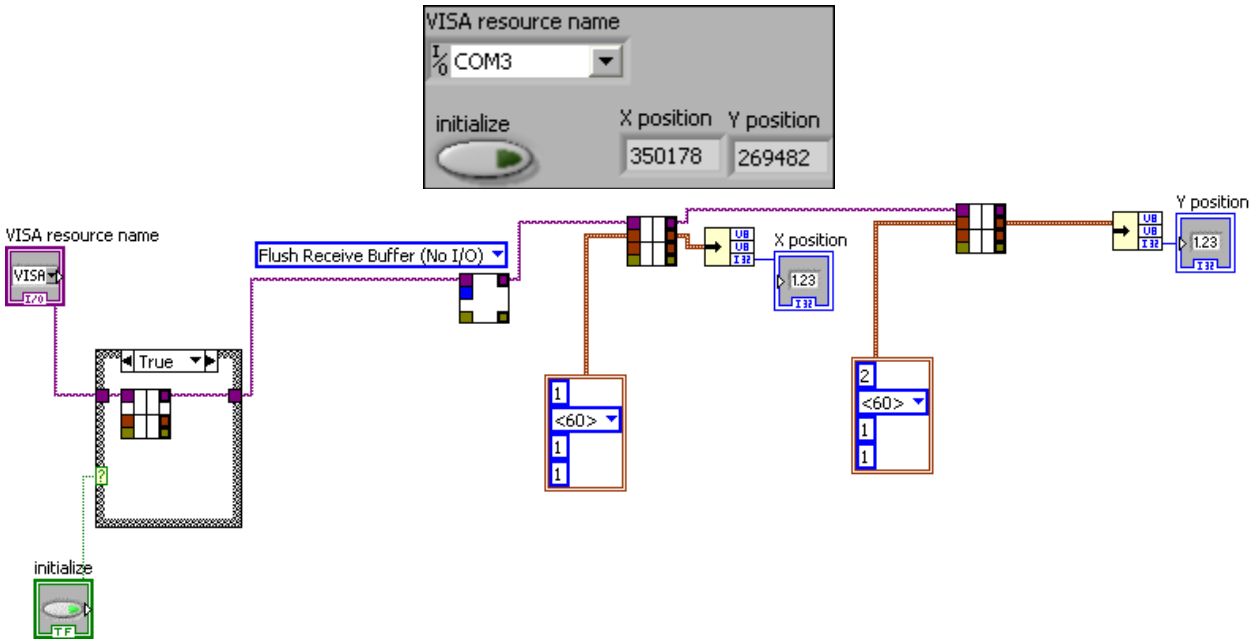

MicroPL front panel:

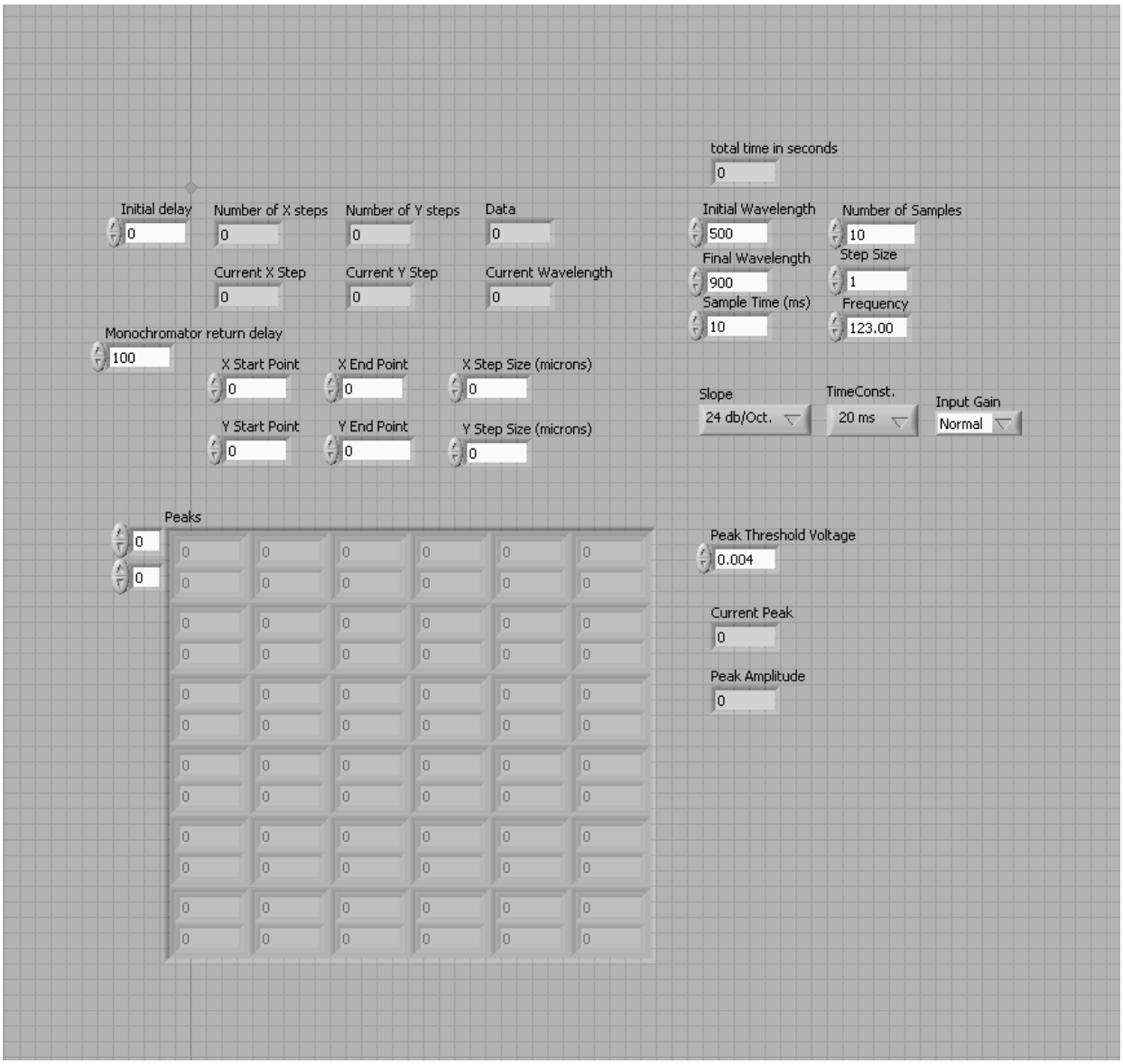

MicroPL Block Diagram (part 1 of 4):

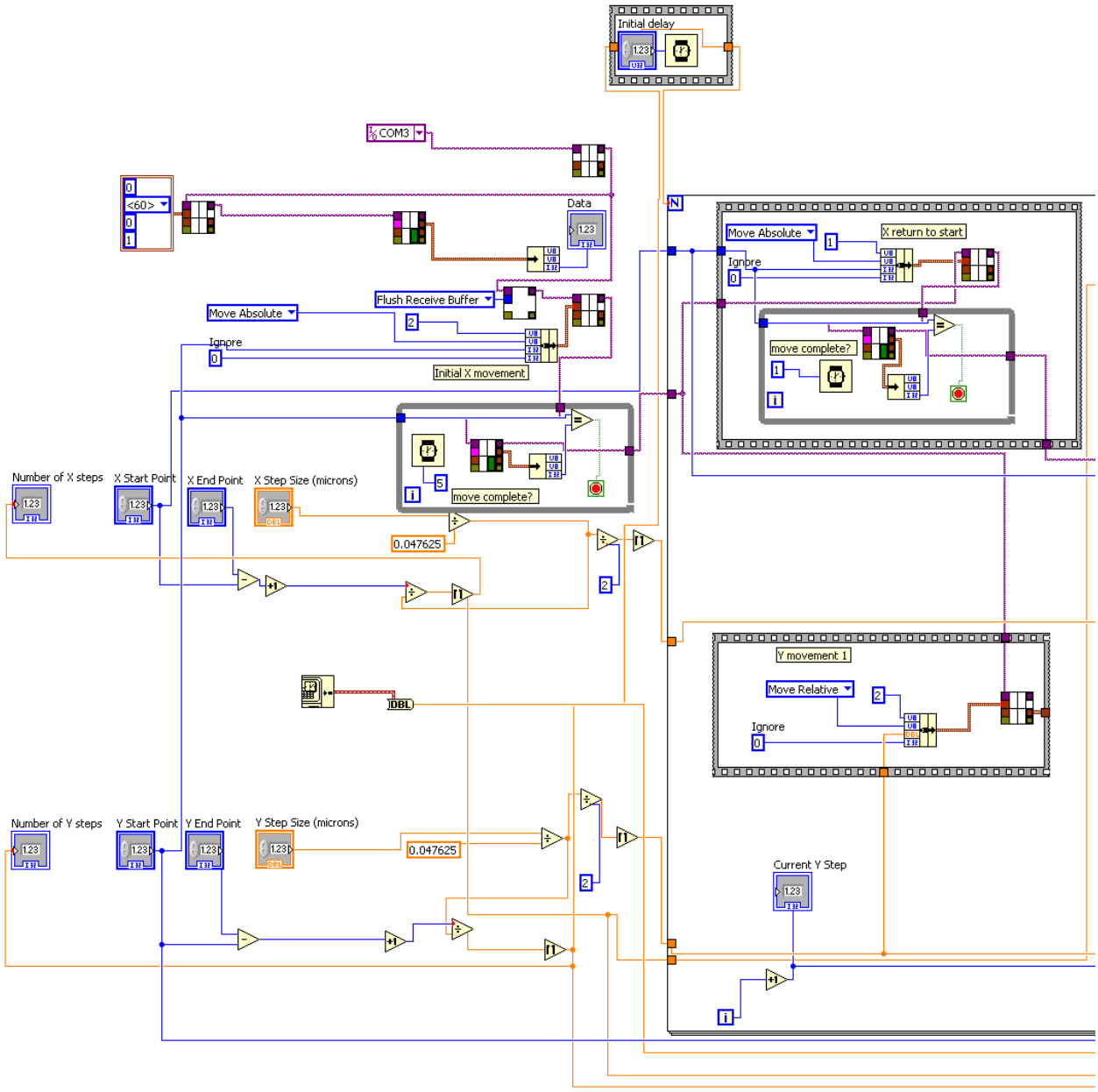

MicroPL Block Diagram (part 2 of 4):

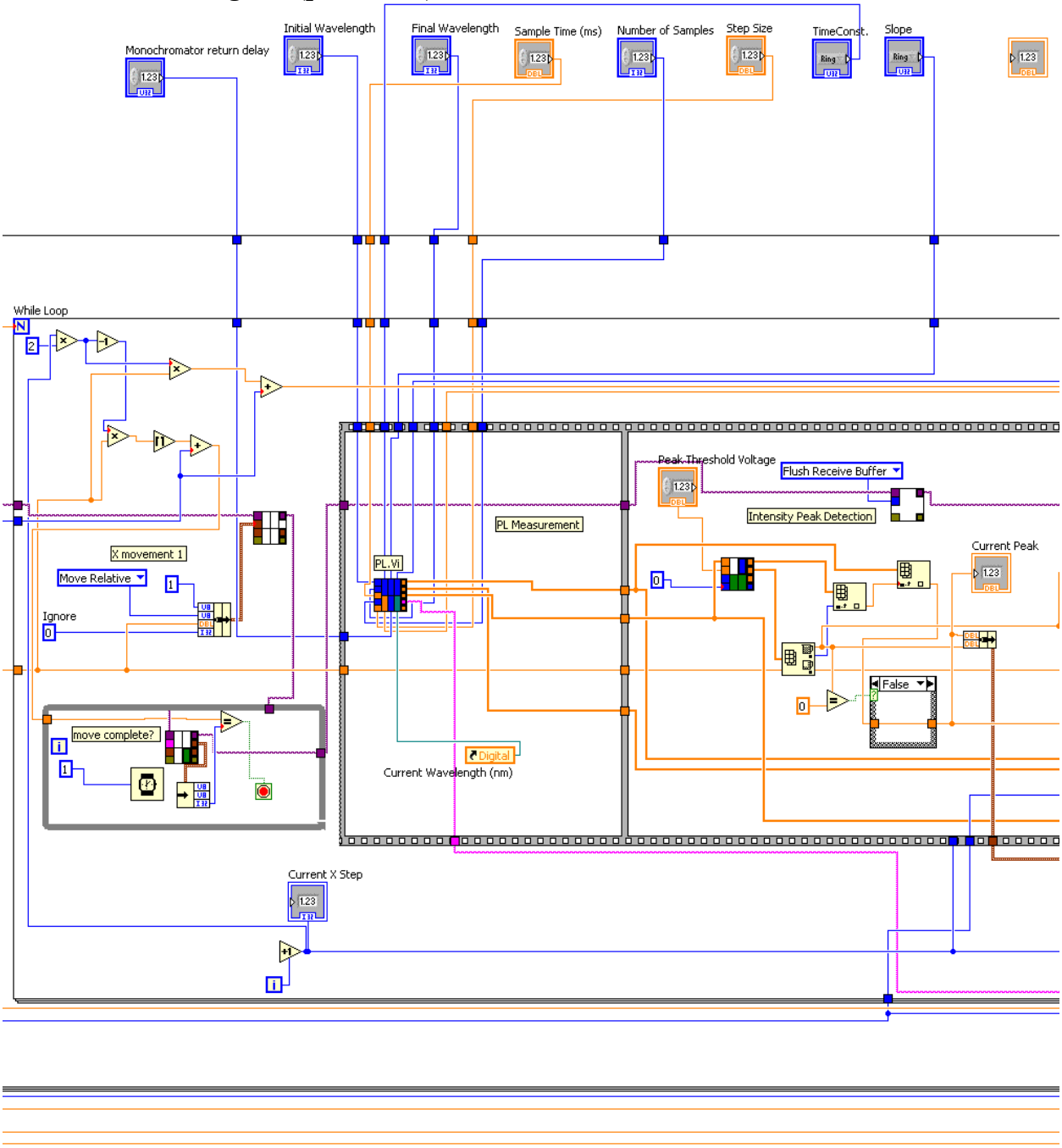

MicroPL Block Diagram (part 3 of 4):

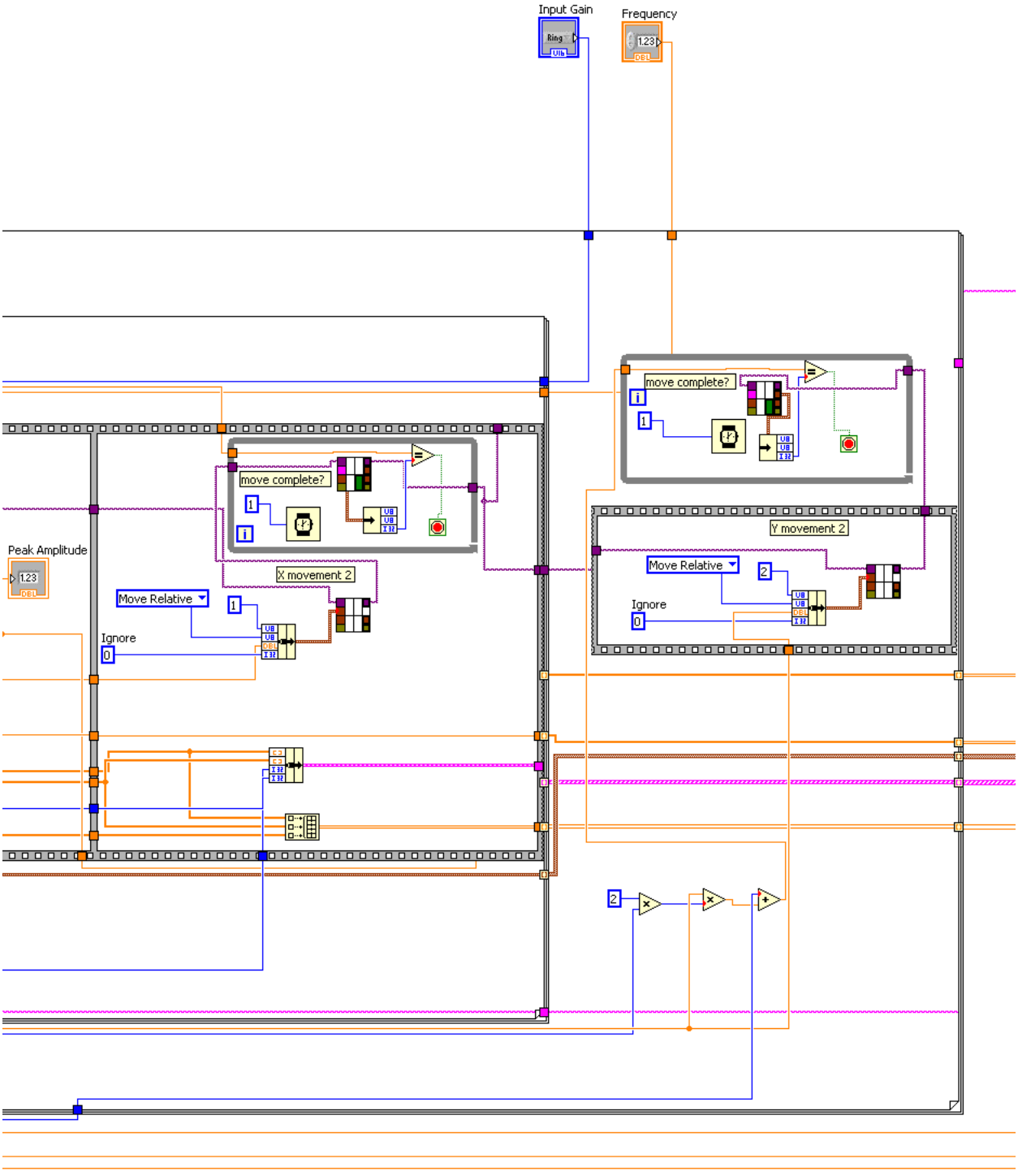

MicroPL Block Diagram (part 4 of 4):

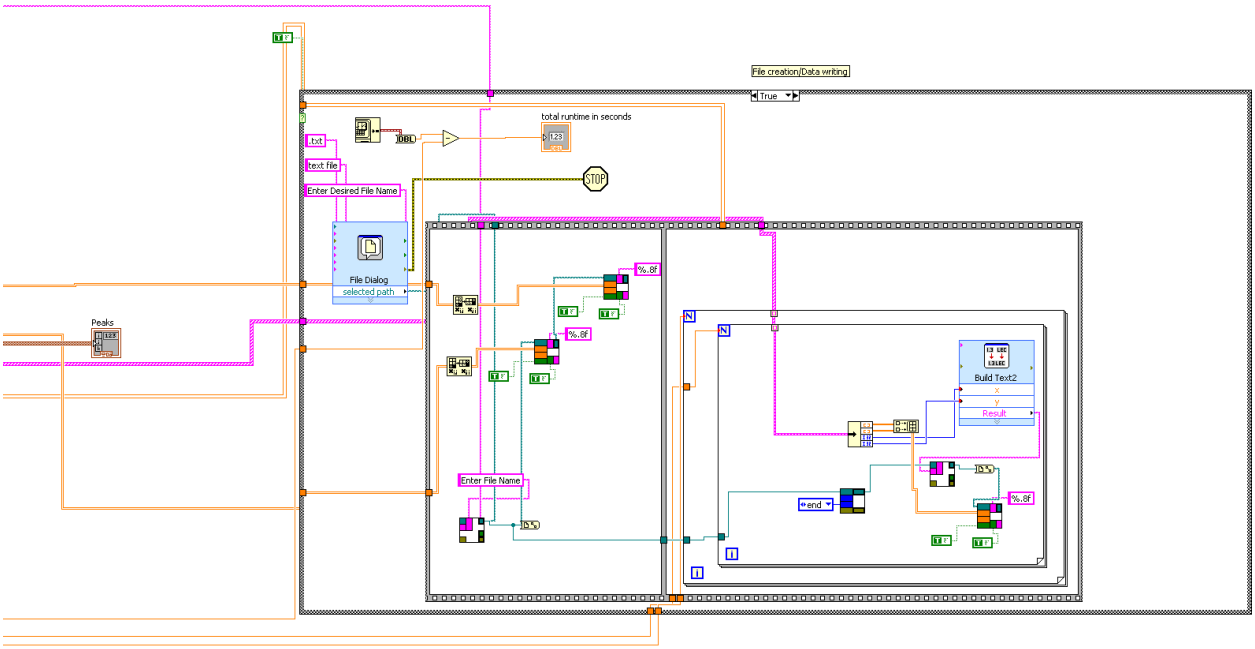

Inputs and outputs for PL.Vi (standard PL code modularized and located in microPL code – see microPL code part 3 of 4) are shown below, with inputs on the left and outputs on the right.

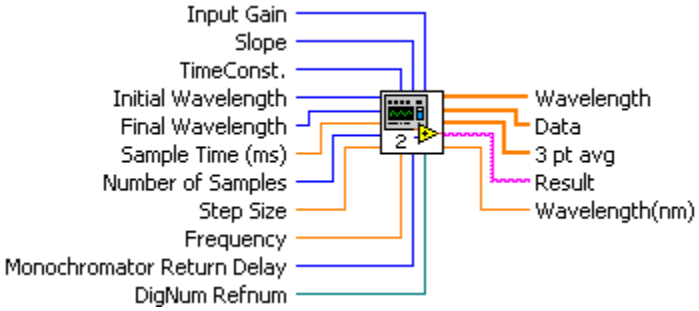

Bibliography

[1] Charles Kittel, *Introduction to Solid State Physics:*, 8th ed. Hoboken, NJ: John Wiley & Sons, 2005.

[2] E. Olsen and a. S. Flø, "Spectral and spatially resolved imaging of photoluminescence in multicrystalline silicon wafers," *Appl. Phys. Lett.*, vol. 99, no. 1, p. 011903, 2011.

[3] T. H. Gfroerer, "Photoluminescence in Analysis of Surfaces and Interfaces," *Encyclopedia of Analytical Chemistry*. John Wiley & Sons, pp. 9209–9231, 2000.

[4] S. Y. Lim, M. Forster, X. Zhang, J. Holtkamp, M. C. Schubert, A. Cuevas, D. Macdonald, and A. P. Technique, "Applications of Photoluminescence Imaging to Dopant and Carrier Concentration Measurements of Silicon Wafers," no. 2, pp. 1–7, 2012.

[5] K. Böhm and B. Fischer, "Photoluminescence at dislocations in GaAs and InP," *J. Appl. Phys.*, vol. 50, no. 8, p. 5453, 1979.

[6] "Anfatec Measurement Unit AMU 2.4 PCI Bus Locking Amplifier 1 Hz to 1 Mhz," vol. 49, no. 0. Anfatec Instruments, Oelsnitz /Vogtland, Germany, pp. 1–32, 2009.

[7] "Visible & IR Femtowatt Photoreceivers, Models 2151 & 2153," no. 408. New Focus, San Jose, CA, 2002.

[8] J. M. Lerner and A. Thevenon, "Section 2: Monochromators and Spectrographs." Horiba Scientific, 1988.

[9] "Digikröm CM110/CM112 Monochromator/Spectrograph," no. August. Spectral Products, Albuquerque, NM, pp. 1–38, 2006.

[10] "Bestform Laser Lens Theory." Special Optics, Wharton, New Jersey.

[11] "Helium-Neon Laser Heads: 1100 Series." JDSU, 2010.

[12] "Gaussian Beam Optics," *Newport Optics*. Newport Optics.

[13] F. L. Pedrotti, L. S. Pedrotti, and L. M. Pedrotti, *Introduction to Optics*, Third Edit. San Francisco, CA: Pearson Addison Wesley, 2007, p. 622.

[14] "Miniature Motorized Linear Stages with Built-in Controllers." [Online]. Available: https://www.zaber.com/products/product_group.php?group=T-LSM&tab=Series Specs#tabs.

[15] T. M. Niebauer, J. E. Faller, H. M. Godwin, J. L. Hall, and R. L. Barger, “Frequency stability measurements on polarization-stabilized He-Ne lasers.,” *Appl. Opt.*, vol. 27, no. 7, pp. 1285–9, Apr. 1988.

[16] G. Yang, a. E. Bolotnikov, Y. Cui, G. S. Camarda, a. Hossain, K. H. Kim, R. Gul, and R. B. James, “Low-temperature spatially resolved micro-photoluminescence mapping in CdZnTe single crystals,” *Appl. Phys. Lett.*, vol. 98, no. 26, p. 261901, 2011.

[17] T. Trupke, R. a. Bardos, M. C. Schubert, and W. Warta, “Photoluminescence imaging of silicon wafers,” *Appl. Phys. Lett.*, vol. 89, no. 4, p. 044107, 2006.

[18] S. Materials, “Band Gap Narrowing Effects in Carbon Doped GaAs,” vol. 3, pp. 1099–1102, 1999.